Two-dimensional quantum hydrogen atom in circularly polarized microwaves: Global properties

Jakub Zakrzewski,[1,2] Robert Gębarowski,[1,*] and Dominique Delande[2]
[1]*Instytut Fizyki Mariana Smoluchowskiego, Uniwersytet Jagielloński, ulica Reymonta 4, 30-059 Kraków, Poland*
[2]*Laboratoire Kastler-Brossel, Université Pierre et Marie Curie, T12, E1, 4 place Jussieu, 75252 Paris Cedex 05, France*
(Received 21 July 1995; revised manuscript received 23 February 1996)

The ionization of hydrogen Rydberg atoms by *circularly* polarized microwaves is studied quantum mechanically in a model two-dimensional atom. We apply a combination of a transformation to the coordinate frame rotating with the field, with complex rotation approach and representation of the atomic subspace in a Sturmian-type basis. The diagonalization of resulting matrices allows us to treat exactly the ionization of atoms initially prepared in highly excited Rydberg states of principal quantum number $n_0 \approx 60$. Similarities and differences between ionization by circularly and linearly polarized microwaves are discussed with a particular emphasis on the high-frequency regime and on the localization phenomenon. The dependence of the ionization character on the initial state (circular, elliptical, or low angular momentum state) as well as on the helicity of the polarization is discussed in detail. It is shown that, in the high-frequency chaotic regime, close encounters with the nucleus do *not* play a major role in the ionization process. [S1050-2947(96)11406-2]

PACS number(s): 32.80.Rm, 42.50.Hz, 05.45.+b, 34.50.Gb

I. INTRODUCTION

The hydrogen atom placed in an external field plays an exceptional role in the studies of quantum-classical correspondence in the vast area of quantum chaos. This system belongs to a small class of problems in this area where accurate theoretical predictions may be confronted with detailed experimental studies. This unique opportunity has led to great progress in understanding the behavior of quantally chaotic systems for which both the experiments and the theory have been providing new ideas and new challenges.

Despite over 20 years of intensive investigations [1], the theory of a highly excited hydrogen atom in the presence of a static uniform magnetic field still brings us unexpected predictions [2]. The ionization of highly excited hydrogen atoms by linearly polarized microwaves (LPM) also has a long history, which began with the pioneering experiment of Bayfield and Koch [3]. As in the previous example, a complete physical picture of the coupled atom-field dynamics in this problem has yet to be reached. The very first model of the ionization process has been launched [4] using Monte Carlo classical simulations, in which the ionization threshold was associated with the onset of classical chaos in the system. Numerous studies performed since this early work treated the problem either classically or quantum mechanically, at various degrees of approximation. At the same time, improved experiments provided a stimulus as well as new puzzles for the theory (for recent reviews of the theory see [5–11]; experimental details may be found in [12–14]).

A typical quantity measured or calculated in the ionization problem is a microwave field amplitude (called the ionization threshold) required to produce 10% ionization yield as a function of the field frequency for a given duration time of the microwave pulse. Such a definition allows for a rough separation of the microwave frequency domain into a few regions corresponding to different ratios of the microwave frequency ω to the Kepler frequency on the initial orbit ω_K. For the scaled frequency $\omega_0 = \omega/\omega_K \ll 1$, the classical ionization is due to an over-the-barrier escape (as for a static, homogeneous electric field case—the situation realized here in the $\omega_0 \to 0$ limit). Furthermore, in this frequency domain, quantum corrections due to tunneling may be taken into account by means of semiclassical methods [15]. For higher frequencies (but still for $\omega_0 < 1$), the quantum ionization threshold is approximated quite well by the onset of classical chaos and the breakup of Kol'mogorov-Arnol'd-Moser tori. The diffusive gain of energy by the electron is the main mechanism leading to the ionization with some additional modifications due to classical resonances. For frequencies $\omega_0 > 1$, the physics of the ionization is quite different because the quantal thresholds are significantly higher than the estimations of the classical model. This is attributed to the phenomenon of quantum photonic localization, which is analogous to the Anderson localization in disordered solids. Not surprisingly, it is this frequency domain that has been most intensively studied both experimentally and theoretically in recent years [5–9,12–14]. Needless to say, the discrepancy between classical and quantum predictions of the threshold for $\omega_0 > 1$ is of importance for a deeper understanding of the semiclassical limit. Finally, one envisions a ''high-frequency'' domain where a typical multiphoton ionization occurs. Certainly, in this regime, not only ω_0 but also the (purely quantum) number of photons needed to reach the threshold $\mathcal{N}_f$ becomes an important parameter characterizing the system.

The physics of hydrogen atom ionization by *circularly* polarized microwaves (CPM) is much less understood although the first theoretical studies came about 15 years ago [16,17]. The recent sudden growth of interest in CPM ionization is certainly stimulated by the experiments carried out for alkali atoms [18,19]. A number of classical studies

*Present address: Department of Applied Mathematics and Theoretical Physics, The Queen's University, Belfast BT7 1NN, Northern Ireland.

have been reported [20–30]. In most of these works (with important exceptions of Refs. [22,28,30,31]) a simplified two-dimensional (2D) model of the atom has been used; i.e., the electronic motion plane coincided with the polarization plane. Also the only quantum study [32] considered such a simplified atomic model.

The first reason for considering the simplified model is the lesson learned in the LPM ionization studies. There, significant insight into the ionization process has been obtained from the simplest, one-dimensional (1D) atomic model where the electronic motion is restricted to the field axis, the direction along which the external field is the most effective. Similarly, for the CPM ionization problem, the simplest 2D model is to restrict the electronic motion to the plane where the external field acts. While the quantitative predictions obtained using this simplification may differ in particular cases from the full three-dimensional treatment, the 2D model should allow one to gain significant insight into the mechanism of ionization.

There is a basic difference between ionization by the LPM and by the CPM. In the former case, the projection of the angular momentum on the polarization axis is conserved, thus the considered problem is effectively a two-dimensional one. On the contrary, the case of the CPM ionization requires, in principle, studying a fully three-dimensional (3D) system, because no constant of motion is known to exist apart from an approximate one in the purely perturbative regime [33]. Such a 3D quantum study, for initial atomic states with principal quantum number of the order of 50, and covering a broad range of initial atomic states and microwave frequencies, is not possible even with good present-day computer resources. For that reason too, we shall limit the present study to the 2D model, especially since, as mentioned above, most of the classical studies also consider the 2D model.

Following the experiments [18,19], theoretical studies of the CPM ionization concentrated mostly on the low-frequency situation, $\omega_0 < 0.6$, both classically [20,22,24–26,28] and quantum mechanically [32]. The motion in this regime is mainly regular [25,28]. We refer the reader to original works for details since we shall consider here the intermediate- and the high-frequency domains only, an interesting case from the quantum chaos point of view.

The quantum study presented extends our previous analysis of low-frequency ionization [32] into this new frequency domain, the region that has been the object of extensive studies in the last few years. For that reason we present first, in the next section, a short summary of known results for the system studied, results obtained mainly within classical mechanics. Later, in subsequent sections, we present our quantum treatment of the ionization in the CPM, discuss possible approaches to calculate the ionization probability and, in particular, discuss the definition of the ionization threshold. Due to the ambiguities of the commonly accepted microwave amplitude threshold for a fixed pulse duration, we define a measure—a pulse duration threshold for a given microwave amplitude—that we call the time threshold. The main numerical results concerning the ionization thresholds for various initial states are presented in Sec. VI. They are compared with the classically obtained thresholds as well as with the theoretical predictions. We discuss the origin of quantum-classical differences and we show the importance of the time scale over which appreciable ionization takes place. We find also several classically scaling structures in the frequency dependence of the thresholds (Sec. VII). Finally Sec. VIII contains the summary of the obtained results and the conclusions.

II. PRESENT STATUS OF THE UNDERSTANDING OF CPM IONIZATION OF THE HYDROGEN ATOM

Let us begin by introducing the necessary notation. The hydrogen atom in the field of the circularly polarized radiation is described by the Hamiltonian

$$H=\frac{(\vec{p}+\vec{A})^2}{2}-\frac{1}{r} \tag{2.1}$$

with the vector potential $\vec{A}$:

$$\vec{A}(t)=\frac{F(t)}{\omega}[-\vec{e}_x\sin(\omega t)+\vec{e}_y\cos(\omega t)]. \tag{2.2}$$

The electric field reads $\vec{\mathcal{F}}=-\partial\vec{A}/\partial t=F(t)[\vec{e}_x\cos(\omega t)+\vec{e}_y\sin(\omega t)]$ provided $F(t)$ changes slowly with respect to ω^{-1}; $dF/dt \ll \omega F$. Hence $F(t)$ is simply the amplitude of the electric field. In the following we will mainly consider an interaction of atoms with the field of a constant amplitude, $F(t)=F$. Since we assume $\vec{A}$ to be independent of the position (the dipole approximation) the alternative form of the Hamiltonian is obtained in the length gauge:

$$H=\frac{\vec{p}^2}{2}-\frac{1}{r}+F(t)[x\cos(\omega t)+y\sin(\omega t)], \tag{2.3}$$

more commonly met in most of the studies, especially classical ones. Note that a change of the sign of ω in Eq. (2.2) [or in Eq. (2.3)] is equivalent to the change from the right-hand CPM to the left-hand CPM. We shall explore this possibility below and allow ω to take both positive and negative values in order to study both types of polarizations.

One may remove the oscillating time dependence by passing to the frame rotating with the field [34–36], the resulting Hamiltonian is

$$H_R=\frac{\vec{p}^2}{2}-\frac{1}{r}+F(t)x-\omega L_z. \tag{2.4}$$

In the presence of the CPM, the angular momentum projection onto the z axis L_z is no longer conserved. While for a fixed amplitude, the Hamiltonian H_R is time independent, the system possesses no other exact constant of motion, except the energy. The latter is not bounded from below due to the kinetic energy coupling introduced by the L_z term.

It is important to recognize that the energy in the rotating frame is different from that in the laboratory frame. For example, for $F=0$, the degeneracy of the hydrogen atom manifold with energy $E_n=-1/2n^2$ in the laboratory frame is partially removed, the corresponding energies become

$E_n-\omega m$. Note also that the change of L_z into $-L_z$ is equivalent to a change of sign of ω. This symmetry reflects the fact that the fate of the atom initially in a given $|n,l,m\rangle$ state under the influence of the right-polarized microwave (ω positive) is the same as that of the atom in a $|n,l,-m\rangle$ initial state in the field of left-polarized radiation.

Classically the system studied has a scaling property frequently employed to reduce the number of parameters. Classical dynamics depends on two among three parameters of the problem (the initial energy, the frequency, and the microwave amplitude). Typically one sets the initial energy at $E_0=-1/2$ (in the rotating frame), then the microwave frequency for a given initial state n_0 is measured in units of the Kepler frequency, $\omega_0=\omega/\omega_K=\omega n_0^3$, while the microwave amplitude scales as $F_0=Fn_0^4$. Other quantities should be scaled accordingly (e.g., microwave pulse duration), in particular the scaled angular momentum $\tilde{m}=m_0/n_0$, changes between -1 and 1. We shall mostly use the scaled units below.

Already the early studies [16,17] dealing with almost resonant microwaves ($\omega_0\approx 1$) have shown a stochastic character of ionization by CPM. This picture has been further confirmed by the extension of the photonic localization theory [6] to the circularly polarized microwaves. The authors constructed a Kepler map for the system valid for high frequencies and not too large initial-state eccentricities. The analogy between the Kepler map and the standard map allowed the authors to give predictions for the onset of quantum ionization based on the photonic localization theory. Soon, however, Nauenberg showed [21] that the original map of [6] is noncanonical. He proposed a new canonical map, which is valid (in the perturbative regime) also for low eccentricity initial orbits. A different analytical but also perturbative analysis was performed by Howard [23] who, basing on the resonance overlap analysis, stressed the diffusive character of ionization. Although Nauenberg claimed that the motion for nearly circular orbits is ''surprisingly regular,'' Howard found numerically ''important regimes of highly chaotic near-circular orbits'' in agreement with earlier studies [16,17]. Still, his resonance overlap analysis actually diverges for such orbits. This discrepancy between [21] and [23] may be quite easily resolved by close inspection of the papers. While Nauenberg considers circular orbits rotating in the opposite sense to the field rotation (i.e., corresponding to negative ω, i.e., $\omega_0\approx -1$), Howard discusses positive ω only.

The strong sensitivity of the behavior of circular states with respect to the helicity of CPM (the sign of ω) was also observed at low frequencies [24,32]; for intermediate frequencies it was further studied by some of us [30] classically. Large microwave amplitudes are required to significantly perturb (and eventually ionize) the atom on initial circular orbit for $\omega<0$; by comparison much weaker microwaves yield significant ionization for positive ω.

The classical study [30] allows one to also shed some light on the applicability of the 2D model, since both the 2D and 3D ionization thresholds are presented there. Nauenberg [21] pointed out that some orbits in 3D lose their stability earlier than in 2D, which might have important consequences for the applicability of the estimates for the ionization threshold based on the 2D model. Here again, as we understand, Nauenberg's claim is restricted to the circular orbits rotating in the opposite direction to the field. The numerical simulations performed by us [30,38] indicate that for $\omega>0$, 2D and 3D thresholds practically coincide (compare Figs. 1 and 2 of [30]) while for $\omega<0$, orbits inclined with respect to the polarization plane may ionize faster. This indicates that the 2D model predictions for negative frequencies have to be viewed with caution when compared with the 3D real world. On the other hand, since microwave amplitudes necessary to ionize the atom are much larger for negative than for positive frequencies, the 2D model should yield reliable predictions also for the microcanonical sample (atoms with well-defined principal quantum number but not preselected with respect to angular momentum, as in current experiments on the hydrogen atom [13]).

This strong dependence of the ionization character on the initial state indicates that at the microwave field amplitudes in the vicinity of the ionization threshold, the classical phase space is of the mixed type, similarly to the corresponding ionization process in LPM. In the latter case, even the experimental data (obtained with the microcanonical initial ensemble of atomic states) show pronounced classically scaling structures that may be related to remaining regularities in the phase space [8,9,12,14]. Similarly, a strong dependence on the angular momentum of the initial state is predicted [6,37].

This similarity between LPM and CPM has been confirmed in a very recent experimental study [39], which compared the ionization thresholds obtained for $0.5<\omega_0<1.4$. Actually, since the initial atomic sample contained a mixture of different (l,m) states of the same principal quantum number, such an experiment is not sensitive to the helicity, the threshold being due to the (l,m) states that ionize first.

Let us come back to the case of a well-defined initial state. Howard's paper [23] brings an interesting discussion of the phase-space structures. In particular he has found, surprisingly, that some areas of the phase space may be totally forbidden corresponding to nonexistent trajectories with complex eccentricity. In such a situation he predicted that the primary one-to-one resonance should not exist for nearly circular orbits. Unfortunately, this claim must be incorrect since, as early as 1989, Klar [40] found an exact stable periodic orbit lying in the middle of the one-to-one resonance zone analytically (let us note, parenthetically, that a very similar calculation leading to the same results has been repeated by Howard himself [41]). As pointed out by Klar, this orbit, a stable fixed point in the rotating frame (as well as its unstable image on the other side of nucleus), may support well localized quantum states. This idea was further developed in Ref. [42] where it has been shown, by direct integration of the time-dependent Schrödinger equation that a wave packet placed on the orbit does not disperse for at least 20 Kepler periods. Although their finding was soon challenged by others [43] claiming that the classical stability island is too small to support quantum states, recent quantum calculations [44] have not only found the actual quantum states localized on the classical resonance island but also accurately determined their lifetimes due to the ionization. The existence of the wave-packet states (as they are called) has been further confirmed by us in a full 3D quantum calculation [45]. Referring the reader for details to these papers, let us note here only that the results of the fully 3D calculation in

that case are in good agreement with more easily obtained results for the 2D simplified model. This provides an additional argument towards application of the 2D approximation in well chosen cases. It is also worth mentioning that analogous wave-packet states have been found for LPM [46,47], showing again the similarity between LPM and CPM excitation.

It is clear, therefore, that the prediction considering the ''forbidden zone'' [23] is a fallacy based on an inadequate choice of the Poincaré surface of section, rather than a real physical situation. To realize the origin of the error, one should consider the energy in the rotating frame, Eq. (2.4), denoted by K in [23]. While K may take any mathematical value, only those values are physically relevant that may be realized via switching on the microwave amplitude from $F=0$ to a given value of F (during the switching K is not conserved since H_R is time dependent). Numerical simulations performed by us indicate that most of the trajectories starting from the initial circular state end up with K values different from those used by Howard [23] in the region of the phase space where no ''forbidden zone'' exists.

Another point that provoked quite a discussion in the literature concerns the mechanism leading to ionization. Howard [23] claims that all orbits, irrespective of their initial shape ''become elongated before they ionize, demonstrating that core effect must be considered in experiments on Rydberg atoms.'' In the same spirit he states that ''in general, higher eccentricity orbits are more easily perturbed.'' Similar claims may be found in [29]; the authors state that ''ionization occurs through a sequence of close encounters with the nucleus.'' Quite an opposite picture emerges from careful classical simulations performed by some of us [30]. We have found that orbits of medium eccentricity ionize first and have shown explicit examples of trajectories that ionize without apparent change of shape and never coming close to the nucleus. Similar conclusions have been reached in the model of molecular dissociation [48], which under certain approximations reduces to the Hamiltonian equivalent to Eq. (2.4). The discussion that followed [49,50] clearly supports the fact that collisions with the nucleus play a marginal role in CPM ionization. As a matter of fact, the ''exact'' quantum results presented in the following sections indeed prove that close encounters with the nucleus play a minor role only.

To summarize, although the subject is infested with opposing statements and controversies, such as the ones described above in some detail, the following picture of ionization in CPM in the intermediate and high-frequency regimes (i.e., for $|\omega_0| \gtrsim 0.5$) clearly emerges from the earlier studies. The classical ionization proceeds mainly by diffusion through the mixed phase space, resembling to a large extent the case of LPM ionization (note that here, due to conservation of L_z, collisions with the nucleus, necessarily important for states with $m=0$, are excluded for $|m|>0$). Quantally, there exist some strongly localized states, studied mostly in the prominent one-to-one resonance zone. Thus one may expect a quantum slowdown of the ionization process due to the phase-space structures. While the region of one-to-one resonance has been explored in some detail, to our knowledge, no reliable quantum calculations exist in the moderate- and high-frequency regimes that are capable of providing a comparison between the classical and quantum predictions. The aim of this paper is therefore to provide such a comparison, which has already been called for in the controversial paper of Howard [23].

Both the classical simulations [30] and the existing quantum [44,45] results indicate that to get the average trends necessary to characterize the frequency dependence of the ionization threshold, the application of the 2D model of the atom is justified. We shall therefore restrict ourselves to such a model below.

III. THE QUANTUM APPROACH

Let us consider first the two-dimensional model of hydrogen without any external perturbation. Its Hamiltonian (in atomic units) is obtained from the standard three-dimensional case by suppressing the z dependence:

$$H_0=\frac{p_x^2+p_y^2}{2}-\frac{1}{\sqrt{x^2+y^2}}. \tag{3.1}$$

The quantum energies follow the Rydberg formula, $E_n=-1/2n_*^2$, where the effective principal quantum number, $n_*=n+1/2, n=0,1,2,\ldots$, appears rather than n itself. The states may be characterized by two quantum numbers: (n,m), where $m=-n,\ldots,n$ is the eigenvalue of the angular momentum operator $L_z=xp_y-yp_x$.

In the presence of the CPM, we might use the length gauge Hamiltonian, Eq. (2.3); however, it turns out that the velocity gauge is more efficient numerically. Expanding the kinetic energy in Eq. (2.1) and removing the constant A^2 term, one arrives at the Schrödinger equation of the form

$$i\frac{\partial}{\partial t}|\psi\rangle=\left(\frac{p^2}{2}-\frac{1}{r}-\frac{F}{\omega}[p_x\sin(\omega t)-p_y\cos(\omega t)]\right)|\psi\rangle. \tag{3.2}$$

The Hamiltonian in Eq. (3.2) is an oscillatory function of time. Therefore one may use the Floquet theory [51] frequently applied to ionization problems in both the optical and microwave regimes. We adopt here another approach and, as in Sec. II, we remove the oscillatory time dependence by passing to the rotating frame. Under the unitary transformation $U=\exp(i\omega L_z t)$, Eq. (3.2) becomes

$$i\frac{\partial}{\partial t}|\tilde{\psi}\rangle=\left(\frac{p^2}{2}-\frac{1}{r}+\frac{F}{\omega}p_y-\omega L_z\right)|\tilde{\psi}\rangle, \tag{3.3}$$

where $|\tilde{\psi}\rangle=U|\psi\rangle$. Since the Hamiltonian is now time independent, we may look for the eigenvalues and eigenvectors of the corresponding time-independent Schrödinger equation. In the following, we pass to the scaled semiparabolic coordinates defined as $u=\sqrt{(r+x)/\Lambda}$, $v=\sqrt{(r-x)/\Lambda}$, already used successfully in the treatment of the hydrogen atom in a static magnetic field [1,52]. These coordinates allow one to remove the Coulomb singularity and facilitate accurate classical simulations of the problem [22,27,30]. The Schrödinger equation takes the form of the generalized eigenvalue problem:

$$\left(\frac{p_u^2+p_v^2}{2\Lambda^2}-\frac{2}{\Lambda}-\frac{F}{\omega\Lambda}(vp_u+up_v)-\frac{\omega}{2}(u^2+v^2)(up_v-vp_u)\right)|\tilde{\psi}\rangle=E(u^2+v^2)|\tilde{\psi}\rangle. \tag{3.4}$$

All terms in the equation above have the form of a polynomial in coordinates and momenta. This form suggests the use of the harmonic oscillator basis for an efficient diagonalization of the problem. The scale parameter Λ may be chosen at will and is related to the common frequency of oscillators in u and v coordinates. Introducing standard creation and annihilation operators,

$$u=\frac{1}{\sqrt{2}}(a^\dagger+a), \quad v=\frac{1}{\sqrt{2}}(b^\dagger+b), \tag{3.5}$$

$$p_u=\frac{1}{i\sqrt{2}}(a^\dagger-a), \quad p_v=\frac{1}{i\sqrt{2}}(b^\dagger-b), \tag{3.6}$$

allows for a simple calculation of matrix elements in Eq. (3.4). However, the matrix representation of the $L_z=(up_v-vp_u)/2$ operator becomes complex. Therefore, it is more convenient to introduce circular creation and annihilation operators for atomic variables that obey the circular symmetry invoked by the field,

$$A^\dagger=\frac{1}{\sqrt{2}}(a^\dagger+ib^\dagger), \quad A=\frac{1}{\sqrt{2}}(a-ib), \tag{3.7}$$

$$B^\dagger=\frac{1}{\sqrt{2}}(a^\dagger-ib^\dagger), \quad B=\frac{1}{\sqrt{2}}(a+ib). \tag{3.8}$$

Expressed in terms of these operators, L_z reads

$$L_z=\frac{1}{2}(up_v-vp_u)=\frac{1}{2}i(ab^\dagger-a^\dagger b)=\frac{1}{2}(A^\dagger A-B^\dagger B) \tag{3.9}$$

and is diagonal in the circular oscillator basis, $|n_A,n_B\rangle$. The meaning of the scale parameter Λ is now clear. By choosing $\Lambda=n$ in the absence of the microwave field, one notices that the state $|n_A,n_B\rangle$ is an eigenvector of the Hamiltonian corresponding to the energy $E=-1/2(n+1/2)^2-m\omega$, where $m=\frac{1}{2}(n_A-n_B)$ and $n=\frac{1}{2}(n_A+n_B)$ [53]. Therefore, this is the eigenstate of the field-free 2D hydrogen in the rotating frame. The oscillator basis is equivalent to the so-called Sturmian basis in the original Cartesian coordinates with Λ being the parameter of the Sturmian basis (for the detailed discussion, see [52]). The basis set, for arbitrary Λ, will be denoted as $\{|n,m\rangle_\Lambda\}$. It is a discrete basis that includes exactly the coupling to the atomic continuum.

In the chosen basis $\{|n,m\rangle_\Lambda\}$ the relation of the eigenvalues E_i and eigenvectors $|\tilde{\psi}_i\rangle=\Sigma_{n,m}a_{nm}|n,m\rangle_\Lambda$ of Eq. (3.4) to Floquet eigenstates becomes transparent. In the laboratory frame the i eigenvector becomes

$$|\psi_i(t)\rangle=\exp\{-iL_z\omega t\}|\tilde{\psi}_i\rangle=\sum_{n,m}a_{nm}\exp\{-im\omega t\}|n,m\rangle_\Lambda. \tag{3.10}$$

Indeed, Eq. (3.10) shows a periodic time behavior characteristic for a Floquet eigenstate. It may be verified after straightforward algebra [38] that, starting from the usual Floquet Hamiltonian [51] corresponding to Eq. (3.2) and passing to the similar oscillator representation, one obtains the Floquet matrix in the oscillator-Floquet basis $\{|n,m\rangle_\Lambda|K\rangle\}$ (K enumerates the photon blocks), which has a block diagonal structure due to the selection rule, $m+K=M=\text{const}$. Eigenvalues of different M,M' blocks differ by the value $(M-M')\omega$, as in a typical periodic Floquet structure. Therefore, the diagonalization of Eq. (3.4) is equivalent to finding all independent eigenvalues and eigenvectors of the Floquet Hamiltonian. However, the above-mentioned selection rule appears only in the circular polarization and it is a direct manifestation of the well-known $\Delta m=1$ selection rule for the absorption of a circularly polarized radiation. This rule is still valid for our Sturmian basis $\{|n,m\rangle_\Lambda\}$ since it has the same angular properties as the usual atomic wave functions.

In the presence of an electromagnetic field, the system supports no bound states but rather resonances, due to the coupling to the continuum. To find these resonances and the corresponding wave functions, we use the well-known complex rotation technique [54]. In short, one rotates the coordinates and momenta according to $\vec{r}\rightarrow\vec{r}\exp(i\theta)$, $\vec{p}\rightarrow\vec{p}\exp(-i\theta)$. The matrix representing the Hamiltonian in Eq. (3.4) then becomes complex symmetric and explicitly dependent on the rotation angle θ. The rotation does not affect energy values of the bound states while rotating structureless continua by the angle 2θ in the complex plane. Provided the rotation angle is not too small, the resonances in the continuum become ''exposed'' by the rotation and appear as complex eigenvalues $\epsilon_i=E_i-i\Gamma_i/2$. For a sufficiently large basis set, an interval of θ values exists for which positions of resonances in the complex plane are independent of the rotation angle and the scale parameter Λ. Consequently, E_i is interpreted as the resonance position and Γ_i as its width (the inverse of its lifetime). Moreover, the corresponding wave functions are square integrable.

The diagonalization of Eq. (3.4) yields *exact* (within numerical errors) eigenvalues and eigenvectors of the hydrogen atom coupled to the monochromatic electromagnetic field, i.e., the eigenstates of the atom dressed by the field (Floquet eigenstates) for a given value of the microwave amplitude F. Such a fairly standard approach to treat nonperturbatively the ionization of hydrogen atoms driven by a periodic wave, originates, as far as we could trace, from the work of Chu and Reinhardt [55], and has been used intensively for both the linearly and circularly polarized radiations [56,57]. However, these studies were mostly related to the ionization from

low-lying atomic initial states. In the microwave regime, the same technique was adopted for the LPM by Buchleitner and Delande [9–11] for both 1D and fully 3D situations (effectively 2D due to conservation of L_z — see the Introduction). Our contribution to the method includes its adaptation for the 2D hydrogen atom in the CPM, and also the application of a simple algebra of harmonic oscillators, which allows for an efficient and straightforward matrix evaluation.

IV. IONIZATION PROBABILITY

In the case where the amplitude changes in time, results obtained for various F values correspond to instantaneous dressed states. Clearly, finding the Floquet states does not provide the exact solution of the full time-dependent Schrödinger equation for arbitrary microwave pulse $F(t)$. Two possible ways of generating an approximate solution out of the results obtained for diagonalizations of the Floquet matrix are used quite commonly.

First, let us assume that the atom is in a state $|\varphi_0\rangle$ before the microwave radiation is turned on. For sufficiently slowly varying microwave pulse $F(t)$, the atom has enough time to adjust to the changes in field amplitude—this is nothing but the adiabatic approximation. Under this approximation, it is sufficient to follow the single dressed (Floquet) state, which is a smooth continuation of the initial state $|\varphi_0\rangle$. Such an approach will be referred to as a single Floquet state approximation (SFSA). The energy of the state and its width change with $F(t)$, providing in this way the information about the nonresonant decay of the atomic population to the continuum. Therefore, the probability of ionization after the microwave pulse of a duration T is given simply by

$$P=1-\exp\left\{-\int_0^T \Gamma[F(t)]dt\right\}, \tag{4.1}$$

where Γ is the width of the important single Floquet state.

In the presence of quantum resonances (between field-shifted states) a real population transfer to other states may occur and the SFSA becomes questionable. Such resonances appear as avoided crossings between energy levels as $F(t)$ changes in time. It is well known from the Landau-Zener theory that even in the presence of avoided crossings, the single-state approximation may work in two extreme cases, either for a very slow adiabatic passage or for a fast diabatic passage. The characteristic time scale is set by the inverse size of the avoided crossing gap (minimal distance between levels), $\tau=1/\Delta\epsilon$. If a change in F sufficient to pass the avoided crossing occurs in time Δt, then the adiabatic passage is realized for $\tau\ll\Delta t$. The diabatic transition occurs in the opposite limiting case, i.e., for very narrow avoided crossings.

It is now apparent that the relative sizes of avoided crossings encountered during changes of $F(t)$ are very important. For classically regular systems, the avoided crossings are generically much smaller in size than the mean level spacing. Thus, in the semiclassical limit, one expects that the SFSA can work for the classically regular regime in the situation where avoided crossings are passed diabatically while, in between subsequent avoided crossings, the single level is adiabatically followed (since the size of a typical avoided crossing is much smaller than the mean level spacing). Such a mixed adiabatic-diabatic picture has been commonly assumed for the ionization from low-lying states [56,57]. Here we relate it to the character of the classical dynamics in the semiclassical limit appropriate for the microwave ionization from highly excited initial states.

On the other hand, for classically chaotic systems, avoided crossings of arbitrary size appear abundantly in a typical spectrum [58]. Thus, one expects a breakdown of the SFSA when the ionization is classically chaotic. In exceptional cases, for initial states being strongly localized (on the classical structures in phase space), the SFSA may still work satisfactorily. Its unpleasant feature is, however, that little control over the buildup of the error is possible, except by comparison with the direct time-dependent solution of the Schrödinger equation. Typical microwave pulses used in experiments [12–14,59–62] have a time duration ranging from a few hundred up to thousands of field cycles. For such long times, a direct integration of the time-dependent Schrödinger equation is not feasible. In most of the experimental setups, the microwave pulse has the ''flattop'' shape (with turn-on phase, constant F amplitude dominant phase, and the pulse turn off). Hence it is reasonable to model this situation by a rectangular pulse of a constant amplitude F during the pulse duration T [9]. In this rectangular pulse shape approach (RPSA), a single diagonalization is enough to obtain the ionization probability as

$$P=1-\sum_i \mathrm{Re}(\langle\tilde{\psi}_i|\varphi_0\rangle^2)\exp(-\Gamma_i T), \tag{4.2}$$

where the sum is over dressed states. The scalar product should be calculated without complex conjugation (as appropriate for complex symmetric matrices). As discussed in detail by Buchleitner [9,11], this expression is exact in the limit of long microwave pulses after averaging over the initial phase of the microwave field.

The RPSA, Eq. (4.2), may only partially approximate the real physical processes where the pulse changes smoothly in time. Still one expects this approach to work quite well for a chaotic system when the classical ionization is mainly diffusive. In that case, the actual wave function, e.g., in the ''flattop'' region of the pulse, is a linear combination of many Floquet states; i.e., its span on the dressed eigenbasis is large [63]. Clearly, in such a situation the application of the SFSA is invalid. As discussed in the resonance overlap analysis by Howard [23] and shown numerically [30] in the intermediate- and high-frequency regimes we are interested in, the classical ionization has mainly a diffusive chaotic character. Thus, the use of the RPSA seems to be the only possible computational approach in this region.

V. THE IONIZATION THRESHOLD

Experimental results are typically plotted [12–14] using the scaled variables (see Sec. II). We shall follow the same convention, adapted to the 2D model: n_* rather than n itself is appropriate for scaling. Namely, we use $\omega_0=\omega n_*^3$ and the scaled microwave amplitude $F_0=Fn_*^4$ to characterize the ionization process. Similarly, pulse duration will be measured directly in the number of cycles of the microwave

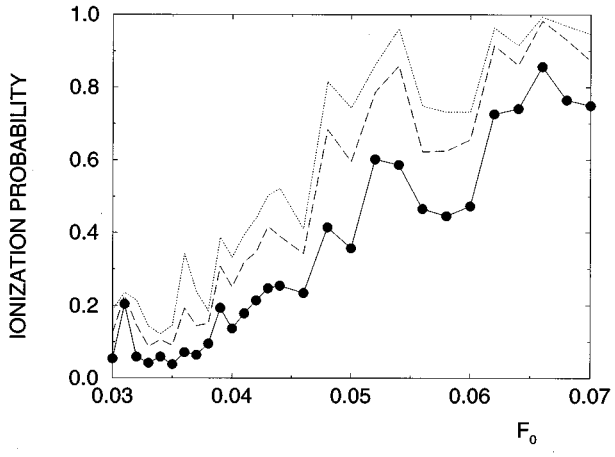

FIG. 1. Probability of ionization at scaled frequency $\omega_0=1$ as a function of the scaled microwave amplitude F_0 for the circular state $|24,24\rangle$ for the duration of the rectangular pulse $T=500$ microwave cycles (filled circles connected by solid line), $T=2000$ (dashed line), and $T=5000$ (dotted line). Note the abundance of local maxima of the ionization curve as a function of F_0.

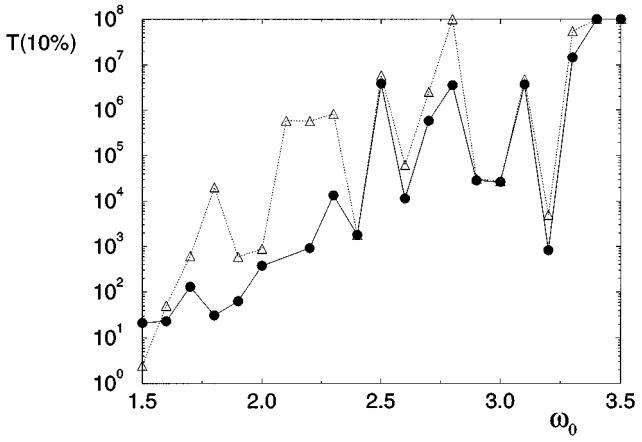

FIG. 2. Comparison of SFSA (open triangles) and RPSA (filled circles) for the circular state $|24,24\rangle$ in the $T(10\%)$ (time) threshold vs scaled frequency ω_0 at scaled microwave field $F_0=0.1$. Note the strong discrepancy between the two approaches for low frequencies (short times) with better agreement for high frequencies and long $T(10\%)$.

field. Results represented in the scaled variables allow for a direct comparison of data obtained for initial states with different principal quantum number. Since the scaling is not preserved quantum mechanically, the experimental and theoretical results for the ionization yield depend on the initial state for the same scaled parameters—this difference should, however, vanish in the classical limit.

The commonly accepted definition of the ionization threshold is the so-called amplitude 10% threshold, $F(10\%)$, i.e., the value of the microwave amplitude for which 10% of atoms become ionized. The dependence of the $F(10\%)$ threshold on scaled frequency ω_0 proved to be a useful characteristic [12]. Recently, such curves showing changes of the $F(10\%)$ versus ω_0 have been extensively studied classically for the CPM ionization [30] for various initial orbits characterized by their eccentricities.

On the other hand, the amplitude threshold $F(10\%)$ is unfortunately quite an ambiguous measure in theoretical studies. The ionization yield is not a monotonic function of F as exemplified in Fig. 1 where we present the yield as a function of the microwave amplitude F for rectangular pulses of different durations. The essential point is that for any pulse duration, several F_0 may yield the same ionization probability. As shown in the figure, the local maxima and minima occur for different probability values, so a simple change from 10% to, say, 50% ionization does not help. This feature is not typically observed in the experiment due to variations of the amplitude with respect to the cavity axis as well as other effects that smear out most of the structures. The nonmonotonic ionization probability dependence on F may be linked to the influence of avoided crossings, as discussed in detail in [10,63,64] and is not an artifact of the approach used (a similar nonmonotonic behavior often termed ''stabilization window,'' is found in ionization studies by strong short laser pulses [65]).

From the theoretical point of view, it is advantageous to have an unambiguous definition of the threshold. It directly follows from the ionization probability formula, Eq. (4.2), that the ionization probability is a strictly monotonic function of the pulse duration T (the realistic values of the field amplitude are orders of magnitude smaller than those needed for a saturation of bound-free transitions, which may lead to Rabi-like oscillations and a nonmonotonic time dependence). We therefore propose and hereafter use mostly the definition of the 10% threshold defined as a pulse duration $T(10\%)$ (in microwave cycles) for which the 10% ionization probability is obtained for given values of the scaled frequency and the microwave amplitude.

The time threshold has additional advantages, both practical and of fundamental interest. The latter, as we shall exemplify below, stems from the fact that the classical-quantum correspondence strongly depends on the pulse duration. This is an aspect of the problem that remained almost unexplored in most of the studies of the microwave ionization (see, however, Refs. [27,59–62]). In practical terms, the time 10% threshold is advantageous because it is much easier to find than the field 10% threshold. In order to determine the 10% time threshold for a given initial state, frequency, and microwave amplitude, it is sufficient to perform only a single diagonalization. This should be compared with several attempts at different F_0 values required to estimate the amplitude 10% threshold. Since initial principal quantum numbers of the order of 50 or more are used experimentally, the corresponding matrices are quite large (see below) and a search for the amplitude threshold becomes very CPU time expensive. We present below both the $T(10\%)$ as well as traditional $F(10\%)$ thresholds; in the latter case the attempt has been made to smooth the nonmonotonic structures by averaging over a range of field values.

An example of the time threshold $T(10\%)$ is presented in Fig. 2, for the same ''testing'' case of the circular state as in Fig. 1 for a rectangular pulse of amplitude $F_0=0.1$. Here, we compare also the SFSA to the exact results based on Eq. (4.2). Large differences (sometimes orders of magnitude) between predictions of both methods are present for intermediate ($\omega_0<3$) frequencies where the classical motion is mainly a nonperturbative chaotic diffusion. This exemplifies the fail-

ure of SFSA in this domain. Apart from the resonance structures, to be discussed in detail below, longer and longer pulses are needed to obtain the 10% ionization yield as the microwave frequency is increased. This behavior reflects the similar increase of the corresponding classical curve for the fixed pulse duration [30]. At higher frequency, $\omega_0 > 3$, the agreement between the RPSA and the SFSA is better: this reflects the perturbative character of the ionization in this limit for $F_0 = 0.1$ (the overlap of the initial state on the most important Floquet state is larger than 0.92) and the quite regular classical dynamics [30].

At this value of F_0, pulses shorter than 100 microwave cycles suffice to yield 10% ionization for $\omega_0 < 2$. On the other hand, for high frequencies, the required pulse duration may well exceed 10^6 cycles. This is an illustration of the fact that, when the atomic response strongly varies with frequency, one should adjust the microwave amplitude to the studied frequency interval so as to remain within a reasonable, experimentally accessible, range of pulse durations. Let us mention that in some experiments [59,62] the pulse duration may be changed by several orders of magnitude.

VI. RESULTS OF NUMERICAL SIMULATIONS FOR A RECTANGULAR PULSE

The results presented up until now served to illustrate our approach and to test possible approximations. They prove that, in the chaotic regime we are interested in, the RPSA is the only possible and at the same time quite a reasonable approximation for long ''flattop'' microwave pulses. To simulate ionization of Rydberg states of principal quantum number $n \approx 60$ typically met in the experiments [12–14,59], the results for $n = 24$ shown above are not truly convincing. In this section, we present $T(10\%)$ thresholds obtained for $n = 48$ and 64, and the comparison with the corresponding classical simulations. It is thus probably a good point now to discuss some technical details of the calculations. A more detailed description can be found in an earlier analysis of the LPM ionization by the same approach [11].

The Sturmian basis $\{|n,m\rangle_\Lambda, \quad n = 0,1, \ldots; \; m = -n, \ldots, n\}$ is complete. However, for practical purposes, we have to limit the size of the basis set. Typically we take the basis vectors up to some $n_{\max}$. In the ideal case (and it was the case for the results presented up until now) $n_{\max}$ should be chosen sufficiently big so that any further increase would not affect the results. The value of the Sturmian parameter Λ is chosen typically in such a way that one of the Sturmian functions coincides with the initial state studied.

Real experiments [12,13] do not measure the absolute ionization yield. Both the stray electric fields present in the experimental setup and the method of detection do not allow one to differentiate between real ionization and excitation of the atom to a very high Rydberg state (with, e.g., principal quantum number $N = 89$ or 114 depending on the experiment [13]). Thus, to simulate a genuine experimental situation, one should count such a high excitation case as ''ionization.'' Fortunately one may use properties of the Sturmian basis to perform such a selection in a very effective and only slightly nonrigorous way as shown in Ref. [11]. Up to a given $n_{\max}$, the Sturmian basis faithfully represents only a finite region of the configuration space. Discrete states that extend further, when represented in the ''too small'' basis, act like continuum states. The effect is clearly seen when diagonalizing the complex rotated atomic Hamiltonian in the absence of any perturbation. The relatively low-lying states are well converged and lie (as they should) on the real axis, the continua are rotated (as they should) by the angle 2θ [54], but the ionization threshold is shifted to smaller energies. It is easy to show (by looking at the Sturmian functions in the coordinate representation [11]) that $N \approx \sqrt{\Lambda n_{\max}}$ is the effective principal quantum number at which the shifted threshold appears. Therefore, limiting the $n_{\max}$ value, one may very efficiently realize a high-N cutoff and at the same time limit the size of diagonalized matrices.

For the atom in a given initial state $|n_0, m_0\rangle$, it is elementary to find out how many photons are required for the ionization in the perturbative picture. Since we are beyond the perturbative limit, it is necessary to include all basis states that may be reached by a few photons more than the minimal required number. Due to the $\Delta m = \pm 1$ selection rule, it is sufficient to form the matrix among the basis states accessible from the initial angular momentum m_0 value by, say, up to K photons, i.e., to restrict the basis states to the interval $m_0 \pm K$. Still the size of resulting matrices may well be up to 25 000. By changing the rotation angle θ and the number of photons K, we were able to verify the convergence of our results.

In order to evaluate the ionization probability, Eq. (4.2), the eigenvalues and eigenvectors that have non-negligible overlap with the initial state are needed. We used the Lanczos diagonalization method adapted for complex symmetric matrices [66], which allows one to obtain a subset of eigenvalues and eigenvectors around a given value of the energy. We started the process around the field-free energy and continued the Lanczos scheme until the eigenvectors found exhausted the norm of the initial state up to 0.995. Typically a small percentage of all eigenvectors was sufficient to satisfy this criterion.

Finally let us describe briefly the classical calculations performed in [30], but with two modifications. First, we have included in the calculations the ''effective threshold'' criterion for the ionization to enable comparison with quantum data. Thus we counted as ''ionized'' any trajectory with final (unscaled) energy greater than $-1/2N^2$. Second, we have determined classically $T(10\%)$ instead of $F(10\%)$ thresholds. The classical results were obtained for a rectangular pulse and for the 2D model of the atom.

As the problem studied is two dimensional, the quantum dynamics is strongly dependent on the geometrical properties of the initial atomic state (in agreement with classical mechanics, similarly sensitive [30]). We cannot discuss all the possible initial states for obvious reasons and we have to restrict ourselves to some illustrative examples. Hence to introduce some systematics into the presentation, first we show results for the elongated states (small m_0) using as an example $m_0 = 0$. Then we consider states of ''average'' ellipticity ($m_0 = n_0/2$), and finally the circular states ($m_0 = n_0$).

A. Elongated states

Let us consider first the minimal angular momentum states, $m_0 = 0$. Such states are extremely important for the

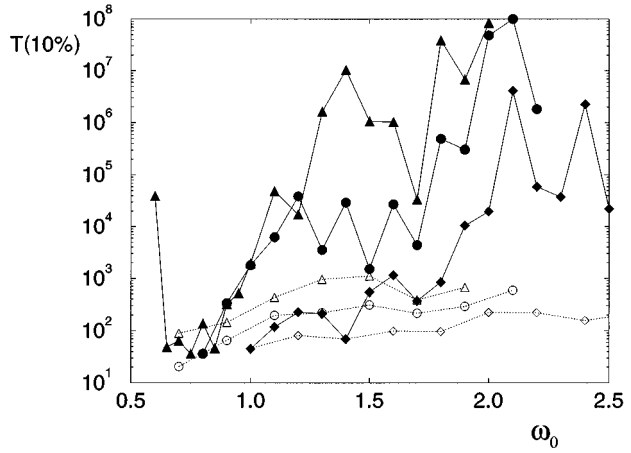

FIG. 3. Length of the rectangular pulse (in microwave cycles) leading to 10% ionization, i.e., the $T(10\%)$ threshold (according to the definition adopted in the text) vs the scaled frequency ω_0 for the initial elongated state $n_0=48$, $m_0=0$ illuminated by a circularly polarized microwave, for different scaled amplitudes F_0. Filled symbols connected by solid lines (to guide the eye) represent the quantum results for the ''effective ionization threshold,'' $N=120$. Open symbols connected by dashed lines give results of classical simulations corresponding to the same effective threshold. Triangles, circles, and diamonds correspond, respectively, to $F_0=0.025,0.03,0.04$.

LPM ionization, where they are most vulnerable to perturbation and among states of different angular momenta, they ionize at lowest amplitudes of the microwave pulse [9–11]. For such states, a simplified 1D model can be used in which the motion of the electron is restricted to the field axis. The behavior of this model has been studied in great detail for the LPM ionization [5–7]. In particular, a lot of attention has been paid to the differences between classical predictions and quantum results; these differences are commonly interpreted as a manifestation of the quantum localization phenomenon, being the quantum chaos analog of the Anderson localization in disordered solids. It is interesting to see whether similar differences are present also for the CPM ionization case.

Figure 3 shows the time $T(10\%)$ thresholds found for moderate frequencies for different values of the microwave amplitude F_0 in comparison with the corresponding classical simulations. For low frequencies, quantum results decrease with frequency (as seen for the smallest amplitude data)—this is a signature of the small frequency behavior studied earlier [24,32] where the motion becomes regular (see discussion in [32]).

For a given scaled field value, the results are presented in the interval of ω_0 where quantum 10% ionization occurs for times between 10 and say 10^8 field cycles. The upper limit is sufficiently high to make experimental verification of our calculations plausible. On the other hand, the resonance widths corresponding to such long interaction times are quite small. They are in fact on the border of the numerical accuracy in the double precision arithmetics. The lines crossing the upper border of the figure indicate the frequency regime in which we could not, for that reason, determine the widths accurately. Since the corresponding $T(10\%)$ are outside the experimental range, they are not of major interest: in such a regime, the atom will be observed as stable against the ionization.

With increasing F_0, the curves typically shift to higher frequencies, indicating that the ionization yield decreases with ω_0 for fixed values of the microwave pulse amplitude and its duration. By comparison, the corresponding classical time thresholds (shown as dotted lines) are almost insensitive to the frequency change in the presented frequency interval shown. In effect, the agreement between the classical and quantum predictions is strongly dependent on the frequency but also, importantly, on the time needed for reaching the threshold. The classical and quantum thresholds agree quite well, especially for low frequencies ($\omega_0<1$), when 10% ionization is reached in less than 100 microwave cycles. At higher frequencies, classical and quantum results differ by orders of magnitude in values of $T(10\%)$.

These results may be confronted with the prediction of the localization theory as based on the so-called Kepler map [6]. The applicability of the Kepler map for the 2D CPM ionization case is limited to the regime

$$\omega_0 \gg 1; \quad |\tilde{m}| = \frac{|m_0|}{n_0} < \left(\frac{2}{\omega_0}\right)^{1/3}, \tag{6.1}$$

where $\tilde{m}=m_0/n_0$ is the scaled angular momentum taking values between -1 and 1 [6]. Clearly, the second condition may be important for elliptical states discussed later. For the present case of $m_0=0$ only the frequency condition is relevant.

If the photonic localization takes place, then the maximal excitation, up to exponential corrections, is given by the localization length (in number of photons) [6],

$$\mathcal{L} \approx 3.33 n_0^2 \mathcal{H}^2 F_0^2 \omega_0^{-10/3}, \tag{6.2}$$

where

$$\mathcal{H} = 1 + \frac{\tilde{m}^2}{2} + 1.09 \omega_0^{1/3} \tilde{m} \tag{6.3}$$

[see Eq. (63) and Eq. (71) of [6] with appropriate identification of symbols; in particular notice the difference of the factor $\sqrt{2}$ in Eq. (6.3) due to the similar difference in the definition of the microwave amplitude]. Now let us assume that F_0 is sufficiently small to limit the excitation to the region below the effective ionization threshold. Hence, due to the photonic localization, the corresponding $T(10\%)$ is almost infinite: for such small fields, 10% ionization is never reached. The increase of F_0 will lead to the decrease of $T(10\%)$ through all orders of magnitude, and finally the other extreme limit (the fast ionization limit) is reached where a significant ionization occurs faster than the time necessary for the localization to build up.

This variation of $T(10\%)$ is thus a sensitive test of the relevance of the localization theory. Curves representing time thresholds over all possible time scales are plotted in Fig. 3. As before, the sharp growth of $T(10\%)$ with frequency and its shift towards higher frequencies with increasing F_0 is in a qualitative agreement with the photonic localization theory [6] and the corresponding decrease of the localization length, Eq. (6.2). It is worth noting that, for the

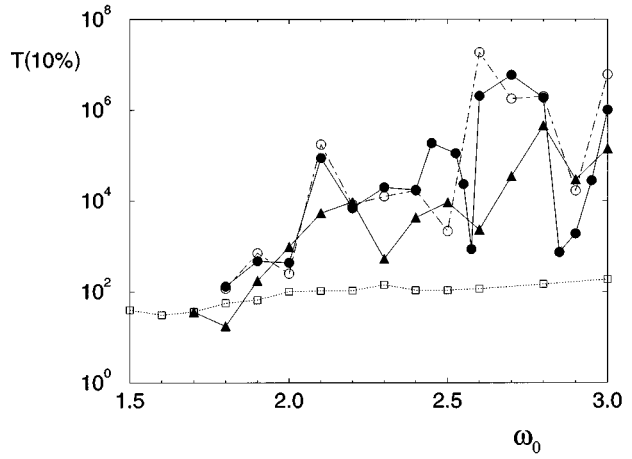

FIG. 4. $T(10\%)$ thresholds for $F_0=0.05$ and elongated state $n_0=64$, $m_0=0$ (triangles connected by line), $n_0=48$, $m_0=0$ (filled circles connected by line), open circles connected by dot-dashed line correspond to threshold obtained for a higher effective cutoff. The results of classical simulations are represented by open small squares connected by dotted line. Possible classically scaling structures appear at $\omega_0\approx 2.1$ and 2.7.

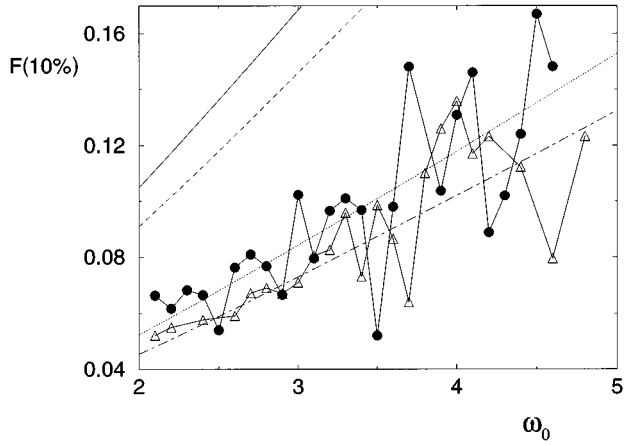

FIG. 5. $F(10\%)$ threshold for the elongated state $n_0=48$, $m_0=0$ ($n_0=64$, $m_0=0$) represented by filled circles (open triangles) as a function of the scaled field frequency (interaction time 500 field cycles). The solid (dashed) line is the prediction of the photonic localization theory [6] and the dotted (dot-dashed) line half this value. The localization theory predicts the correct functional dependence, but with a wrong coefficient.

smallest amplitude $F_0=0.025$ presented in Fig. 3, the increase in $T(10\%)$ due to ''localization'' occurs already for values of ω_0 slightly smaller than unity.

In a typical laboratory measurement or numerical experiment, the variations of the $F(10\%)$ threshold are quite small; they change at most by a factor of 2. On the contrary, the $T(10\%)$ threshold can cover easily a range of several orders of magnitude. This general phenomenon was demonstrated in the LPM [10], but is also observed in our calculations in the CPM. This is simply due to the difference in properties of the measure chosen to define the threshold. Note that the ionization yield is determined by a sum of weighted factors $\exp\{-\Gamma_i(F)T\}$ [in Eq. (4.2)], where widths Γ_i are strongly nonlinear functions of F. A small increase of the microwave amplitude may strongly increase the widths; therefore a necessary decrease of the interaction time so as to keep their product constant may be large. Also, since several terms contribute to the sum in Eq. (4.2), the ionization as a function of time does not follow the exponential rule for the decay out of the initial state; in the classically chaotic regime the decay takes rather an algebraic, much slower character [62]. The sensitivity of the $T(10\%)$ to changes of F_0 suggests it to be a more informative measure of the ionization than the amplitude threshold.

For the sake of further tests of the localization theory predictions, we present the data for stronger fields and higher frequencies in Fig. 4. Again a similar behavior, i.e., the reasonable classical-quantum predictions agreement at lower frequencies with strong disagreement for higher frequencies, is found. Similar results are observed for the higher microwave amplitude $F_0=0.1$ (not shown).

Figure 4 illustrates results for an initial elongated state, $n_0=64$, $m_0=0$. For an appropriate comparison with the classical simulation, we adjusted $n_{\max}$ in such a way that the quantum results for both $n_0=48$ and 64 correspond to the same classical cutoff limit. This is fulfilled when $N=120$ (160) for $n_0=48$ (64), corresponding to $n_{\max}=300$ (400). Note that typically points of $T(10\%)$ for $n_0=64$ are closer to the classical results than those obtained for $n_0=48$. This is expected on semiclassical grounds and is in agreement with the photonic localization theory, which predicts the decrease of the quantum threshold proportional to $n_0^{-1/2}$ [67]. In addition, Fig. 4 shows also data obtained for $n_0=48$ and larger $n_{\max}=480$, corresponding to an effective ionization cutoff $N\approx 151$. While overall results depend weakly on the cutoff value, for some frequencies discrepancies arise. They typically occur when the shift of the cutoff leads to a change in the number of photons needed for the ionization.

A sensitive verification of the photonic localization theory requires a comparison of the *quantitative* predictions of the theory with our numerical results. This is difficult because the photonic localization theory may be used for estimation of the threshold only if the effective threshold is not too high and no significant real ionization occurs (see remarks in the Appendix of [67]). As formulated in [6], the photonic localization theory gives estimates for $F(10\%)$ threshold. In order to test it on a real system, we will focus now on the $F(10\%)$ ionization threshold.

The prediction is [6,67]

$$F(10\%)=\frac{\omega_0^{7/6}}{\sqrt{8n_0}\mathcal{H}}\sqrt{1-\frac{n_0^2}{N^2}}. \tag{6.4}$$

Recall that N is the principal quantum number corresponding to the effective ionization threshold. For elongated states studied in this subsection, $\tilde{m}=m_0/n_0$ is equal to 0 and $\mathcal{H}$ is just equal to 1. Hence, we are left with three parameters: n_0, F_0, and ω_0. First, we fix $n_0=48$ and study the $F(10\%)$ threshold as a function of ω_0. The result in the high-frequency domain is shown in Fig. 5. Apart from the existence of strong fluctuations, there is a general increasing trend with ω_0. The prediction of the photonic localization theory, shown as a solid line, has the same trend but obviously largely overestimates the $F(10\%)$ threshold. The dot-

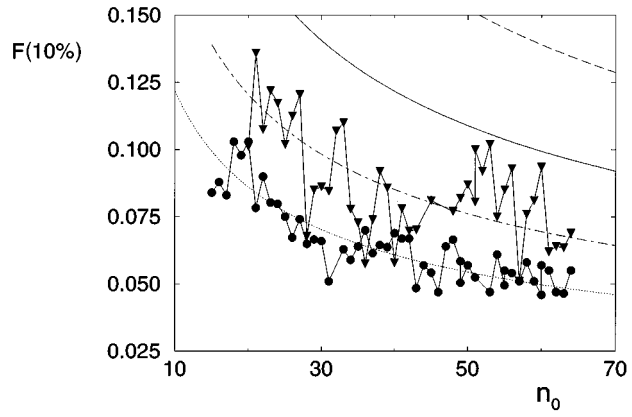

FIG. 6. $F(10\%)$ threshold for the elongated state n_0, $m_0=0$ as a function of the principal quantum number n_0 (interaction time 500 field cycles). Filled circles (triangles) represent the data for scaled frequency $\omega_0=2.1$ ($\omega_0=2.8$). The predictions of the photonic localization theory [6] are shown by solid (dashed) lines while the dotted (dot-dashed) lines give half of the theoretical prediction. The localization theory predicts the correct functional dependence; note that the ''correction factor'' is the same for both frequencies.

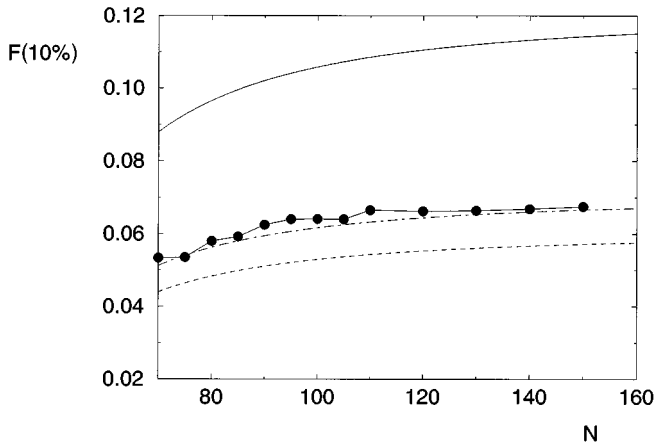

FIG. 7. The dependence of the $F(10\%)$ threshold on the effective ionization threshold N for $n_0=48$ at $\omega_0=2.1$ (filled circles). The prediction of the photonic localization theory [67] is shown by a solid line; the dashed line gives half of this value. The dot-dashed line is a result of a fit of the constant factor in the localization theory prediction to numerical value for large N and in an excellent way describes the variation of the $F(10\%)$ threshold for the whole interval of N values shown.

ted line, equal to half the theoretical prediction, is in good overall agreement with the numerical results. Similar results are obtained for a different initial state $n_0=64$, as is also shown in Fig. 5.

In the second test, ω_0 is fixed and the $F(10\%)$ threshold versus n_0 is plotted. For this purpose, we take $\omega_0=2.1$ and change the size of the basis so that the ratio n_0/N is kept fixed. The result is shown in Fig. 6. Again, the general trend is well predicted by the photonic localization theory (solid line), but the exact value is significantly different. The dotted line is half of the theoretical prediction, and as before it is in good agreement with our data. Quite similar behavior, with the same factor 0.5, is recorded at frequency $\omega_0=2.8$, as is also shown in Fig. 6.

In the third and final test, we fix both ω_0 and n_0 and change only the effective cutoff, N [compare Eq. (6.4)]. The results obtained for $F(10\%)$ are summarized in Fig. 7. As in the previous figures the prediction of the localization theory significantly overestimates the threshold for large-N values; the factor 0.5 improves the agreement considerably. Close inspection of Figs. 5 and 6 reveals, however, that the values of ω_0 and n_0 chosen to coincide with other figures are not the best. At $\omega_0=2.1$ and $n_0=48$, $F(10\%)$ curves in both figures have local maxima, so the factor 0.5 may not work very well. Therefore, we have also attempted to fit the proportionality factor in the $N\rightarrow\infty$ limit. The result, represented as a dot-dashed line, agrees with the numerical data quite well.

Note that while both Fig. 5 and Fig. 6 show quite large fluctuations about the average behavior, these fluctuations are practically absent in Fig. 7. This shows that the origin of fluctuations is not due to the size of the effective cutoff. What is more, the fluctuations are present in the $F(10\%)$ dependence on n_0 (i.e., on the effective $\hbar$), while all classical parameters are kept constant. Thus the fluctuations as a function of n_0 are of a quantum origin. We believe that they are due to quantum interferences between different ionizing paths leading to the continuum and the effect is, to some extent, statistical. Semiclassically the change of $\hbar$ is equivalent to a different level of coarse graining of the phase space, thus these fluctuations may also reflect transport properties from the initial state to the continuum on a changing with n_0 resolution level. Certainly, observed fluctuations deserve a more detailed study, which is, however, beyond the scope of the present paper. Let us mention here only that similar fluctuations are observed [45] for the individual widths of the well-localized so-called wave-packet states (mentioned already in Sec. II) both for the linear and the circular polarizations.

In conclusion, the photonic localization theory is in good qualitative agreement with our numerical results for elongated states. Further work is needed to understand the factor of 2 discrepancy. The numerical value of this factor will be dependent on the pulse duration (note that we use pulses of 500 microwave periods) and it will increase for longer interaction times. Since photonic localization theory is valid, strictly speaking, for infinite interaction times, the appropriate correction factor may be larger. Also, in Eq. (6.3), the factor $\mathcal{H}$ is estimated using the m_0 value of the initial state. However, during the excitation process, the atom absorbs a few circularly polarized photons and the value of m_0 increases. Using a corrected value for m_0 in Eq. (6.3) decreases the prediction of the photonic localization theory by approximately 20% and consequently reduces the observed discrepancy.

Even with this correction, our numerical results cannot be claimed to be consistent quantitatively with the photonic localization theory. The difference factor of 1.8–2 is quite huge and comparable in size to the total difference between the classical simulations and experimental data for LPM in the corresponding frequency regime. There, the localization theory seems to reproduce experimental data in their average trend to much higher accuracy (of the order of 10%). Thus this quantitative failure of the theory for elongated states in

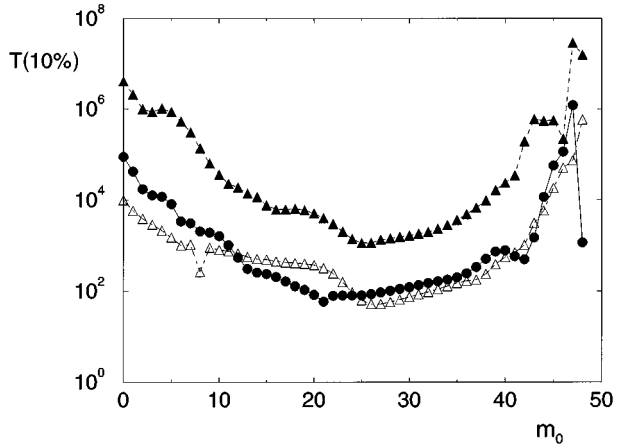

FIG. 8. The dependence of the $T(10\%)$ threshold for ionization on the initial angular momentum m_0 for the $n_0=48$ manifold. The filled (open) triangles correspond to thresholds obtained at $\omega_0=2.1$ and $F=0.04$ ($F=0.05$) while circles present the data for $F=0.04$ and a smaller frequency $\omega_0=1.9$. The lowest threshold values are obtained for $m_0\approx n_0/2$.

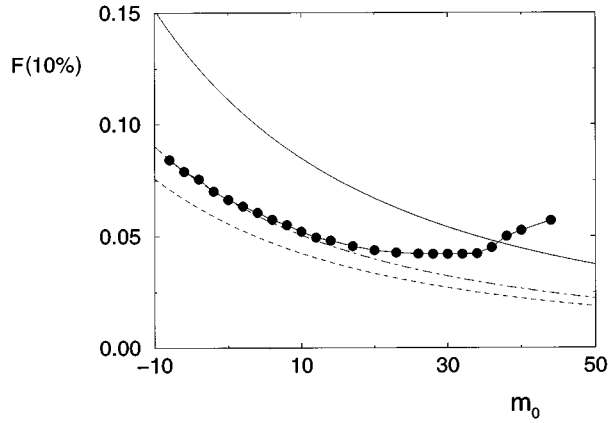

FIG. 9. The dependence of the $F(10\%)$ threshold for ionization on the initial angular momentum m_0 for the $n_0=48$ manifold at $\omega_0=2.1$. The prediction of the photonic localization theory [6] is shown by the solid line; the dashed line gives half this value. The dot-dashed line is a result of a fit of the constant factor in the localization theory prediction to the numerical value at $m_0=0$ and in an excellent way describes variation of the $F(10\%)$ threshold for $|m_0|<10$ (corresponding to scaled angular momentum $|\tilde{m}|<0.2$).

CPM microwaves is quite surprising bearing in mind that Howard classical resonance analysis [23] suggests a close similarity between atomic response to LPM and CPM for elongated states. Again, the failure of this picture may be due to the fact that in CPM, the electron picks up some angular momentum every time a photon is absorbed. This effect is not taken into account in the resonance overlap analysis. As we shall see below in quantum calculations and as already noted in classical simulations [30], states (orbits) of medium eccentricity have the lowest ionization threshold. Thus absorption of photons in CPM, decreasing the eccentricity of initially elongated states, speeds up the classical diffusion. This effect is taken into account only partially by the photonic localization theory.

B. Angular momentum dependence of the threshold

In most of the experiments [12–14], while the initial principal quantum number n_0 is well defined, the atoms are not preselected with respect to the initial angular momentum quantum numbers. This implies that the threshold is dominated by the states ionizing in the smallest microwave field. In the case of the LPM ionization, these are the elongated states. Do these states ionize first also in the CPM ionization? In view of quite opposite pictures emerging from classical calculations [23,30] it is quite interesting to address this issue quantum mechanically.

The quantum results are presented in Fig. 8, which shows, for a fixed value of F_0 and ω_0, the thresholds obtained for all m_0 states in the $n_0=48$ manifold. Notice a broad minimum around $m_0\approx n_0/2$, indicating that indeed elliptical states with moderate m_0 values are most important for the threshold determination in agreement with classical simulations [30]. While the state-to-state inspection of the data reveals a sensitivity of the ionization efficiency on the choice of F_0 and ω_0 values used for the comparison (this is due to the presence of structures in the threshold as a function of ω_0 and the abundance of local maxima in the ionization yield as a function of F_0—compare with Fig. 1), a common overall behavior is observed in a broad range of both F_0 and ω_0.

Such behavior is not unexpected: the classical 1:1 resonance analysis [17,23] shows that the size of the classical resonance island *increases* when the eccentricity *decreases*, indicating that the CPM acts more efficiently when the electron follows a trajectory close to a circle—not a surprising result. However, the same analysis shows that higher-order resonances are less pronounced for low eccentricity. In other words, for states with low eccentricity, the first resonant photons are more easily absorbed, but the following ones are less efficient. It is this balance between the efficiency of the atom-photon interaction (which favors low eccentricity) and nonlinearity (which favors high eccentricity) which is responsible for the observed phenomenon.

The increase of the ionization efficiency with m_0 for a fixed microwave amplitude and frequency is also predicted by the photonic localization theory [6]. For $\omega_0\approx 2$, the angular momentum condition for the applicability of the theory is satisfied for almost all $\tilde{m}$ values, up to $\tilde{m}$ close to 1 (corresponding to circular states). The localization length, Eq. (6.2), is determined by the product of $\mathcal{H}F_0$, where $\mathcal{H}$ increases monotonically with $\tilde{m}$ [compare with Eq. (6.3)]. Thus, for fixed F_0 and ω_0, the localization length increases with $\tilde{m}$. A quantitative test is presented in Fig. 9. The solid line is the prediction of the photonic localization theory, which is greatly different from the numerical data. However, the qualitative trend is well verified (for negative and positive $\tilde{m}$). Correction by a factor 0.5, as before, yields (dashed line) a reasonable agreement with the data. A comparison with Fig. 5 shows that at $\omega_0=2.1$ the fluctuations in the quantum numerical data are not ''favorable'' and the factor 0.5 does not work too well. Therefore, we have fitted the correction factor so that the numerical value and the modified prediction of the localization theory [6] exactly coincide at $\tilde{m}=0$. Such a modification yields a dot-dashed line in excellent agreement with numerical data for $|\tilde{m}|<0.2$.

Two important factors are to be noticed. First, the fluctuations are much smaller than in Figs. 5 and 6. This lack of fluctuations may be explained by correlations between $F(10\%)$ values for close m_0 quantum numbers. The origin of this correlation is mainly classical—the angular momentum in the CPM ionization problem is not conserved and the classical phase space is ''shared'' by different initial m_0 values. The situation is completely different in this respect from a more familiar interaction with the LPM, which conserves m. While paths leading to ionization of various m_0 states are different, which is reflected by the change of $F(10\%)$ with m_0, some correlations between ionization yields for little differing values of m_0 are to be expected. In fact we have verified, by calculating the n_0 dependence of $F(10\%)$ for $m_0=2$ (not shown), that the structures observed in Fig. 6 are exactly reproduced for $m_0=2$, the only difference being the lower average behavior that is consistent with Fig. 9.

Second, the localization theory clearly breaks down around $\tilde{m}=0.5$, whereas the prediction Eq. (6.1) is supposed to be valid everywhere. Obviously, the conditions in Eq. (6.1) are not sufficiently restrictive. As a matter of fact, the Kepler map relies on the approximation that most of the energy exchange takes place in the vicinity of the perihelion. For states with not small angular momentum, this cannot be true. Hence, the applicability of the Kepler map is at best restricted to small angular momentum $\tilde{m}\ll 1$ and high frequency.

Our quantum results are in this respect in good agreement with a classical study of Nauenberg [21] who, as mentioned in the Introduction, constructed a better, canonical map after noting difficulties with the original Kepler map of Ref. [6]. It would be most interesting, therefore, to compare quantum results with predictions of the photonic localization theory based on the canonical Kepler map of Nauenberg instead of the standard Kepler map of [6]. For a high eccentricity, a small microwave amplitude and a high frequency, the Nauenberg Kepler map is close to the standard Kepler map and no significant difference is likely to take place. On the contrary, at medium and low eccentricities the two maps are significantly different. The breakdown of the photonic localization theory around $\tilde{m}=0.5$ may be due to either a breakdown of the classical standard Kepler map or a failure of the localization picture itself. This interesting alternative is left for the future studies since a generalization of the theory of [6] for a map of a different functional form is unfortunately not straightforward. The results presented indicate that some effort should be taken in this direction.

C. Elliptical states

Since states with $m_0\approx n_0/2$ are ''the first to ionize'' among different angular momentum states, it is worthwhile to investigate their properties in more detail. As an example, we have chosen the states $n_0=48$, $m_0=24$ and $n_0=64$, $m_0=32$. Recall that, according to the convention adopted here, positive ω_0 correspond to positive m_0 states in right-polarized microwaves (or $-m_0$ states in left-polarized microwaves). Figure 10 presents the moderate-frequency behavior for the $n_0=48$, $m_0=24$ state. As for the elongated states, one observes the decrease of the threshold with scaled frequency for low frequencies ($\omega_0\approx 0.6$). For higher frequencies, $T(10\%)$ is again an increasing (on average) function of ω_0. Note that the microwave amplitudes F_0 leading to comparable $T(10\%)$ for a given scaled frequency are smaller for elliptical states than those used in Fig. 3. This confirms the fact that elliptical states ionize much faster than elongated states in a broad frequency range. A comparison with the corresponding classical simulation reveals again that for effectively weaker pulses, corresponding to longer $T(10\%)$, the quantum ionization proceeds much slower than its classical counterpart. On the other hand, one may notice, again by comparison between Fig. 3 and Fig. 10, that the classical-quantum disagreement is less pronounced and less sharp for elliptical states than for the elongated states. This is confirmed further in the higher-frequency interval—compare Fig. 4 and Fig. 11.

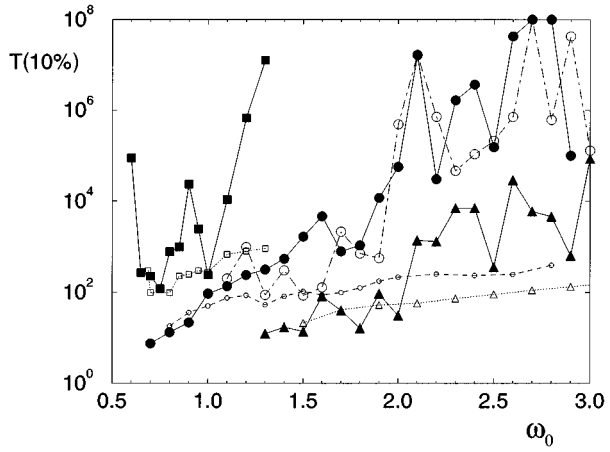

FIG. 10. $T(10\%)$ threshold for elliptical state $n_0=48$, $m_0=24$. The filled symbols correspond to quantum results, while the small open symbols stand for classical simulations. $F_0=0.015$, 0.025, and 0.04 data are represented by squares, circles, and triangles, respectively. The large open circles connected by a dot-dashed line correspond to a higher-lying initial state $n_0=64$, $m_0=32$—comparison with filled circles allows for locating classically scaling structures.

The thresholds obtained for these elliptical states are very comparable (within 10%) to the ones obtained numerically

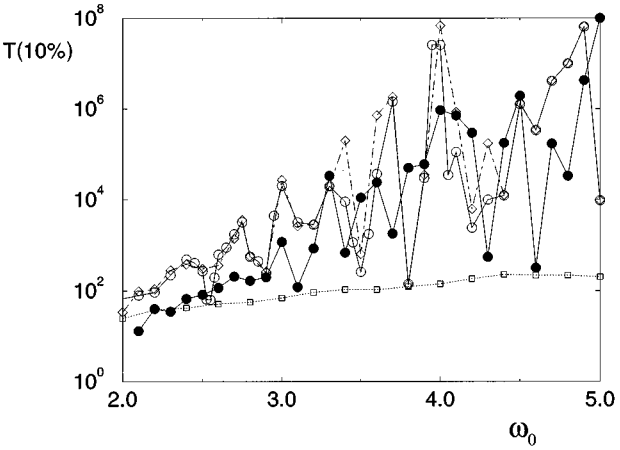

FIG. 11. Same as Fig. 10 but for $F_0=0.05$. Filled circles, $n_0=64$, $m_0=32$; open circles, $n_0=48$, $m_0=24$; diamonds, $n_0=48$, $m_0=24$ for higher effective cutoff; squares connected by a dotted line, classical simulation results.

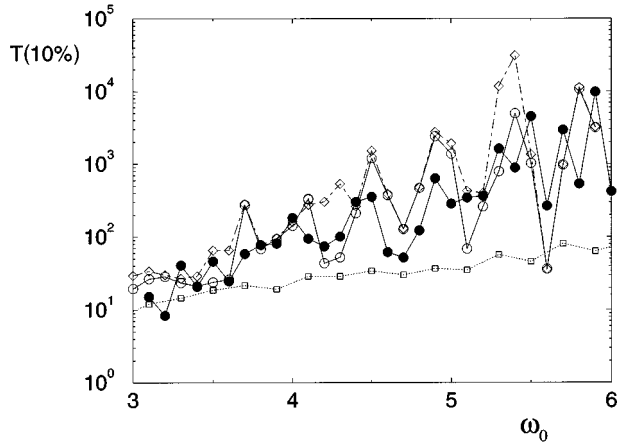

FIG. 12. Same as Fig. 11 but for $F_0=0.1$. Filled circles, $n_0=64$, $m_0=32$; open circles, $n_0=48$, $m_0=24$; diamonds, $n_0=48$, $m_0=24$ for higher effective cutoff; squares connected by a dotted line, classical simulation results.

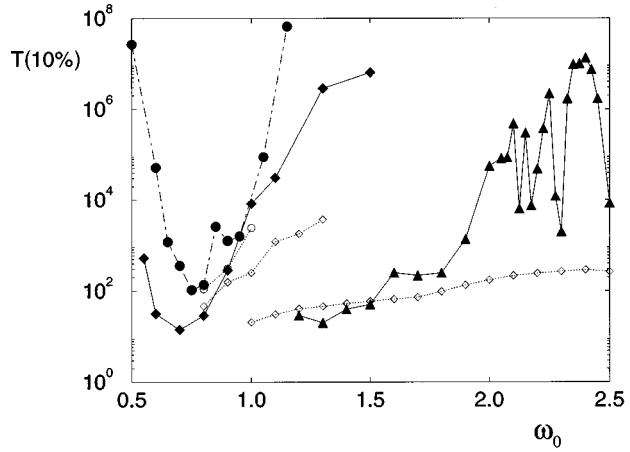

FIG. 13. $T(10\%)$ threshold for the elliptical state $n_0=48$, $m_0=24$ in left-hand CPM (or $m_0=-24$ in right-hand polarized radiation). The filled (open) symbols connected by lines give the quantum (classical) results. The circles, diamonds, and triangles correspond to $F_0=0.04$, 0.05, and 0.1, respectively.

for elongated states in LPM [9,11] at similar frequency and interaction time. They are also in good agreement with the recent experimental results [39] obtained using a statistical ''microcanonical'' mixture of initial states. Our calculations show that the experimentally measured threshold is due to intermediate m_0 states. They also suggest that a significantly higher threshold should be observed using either a pure elongated or circular initial state.

A still higher frequency range is represented in Fig. 12. Note that the overall behavior of the threshold is quite similar to that observed for lower frequencies (and lower field) in Fig. 11. Namely, there is an apparent agreement between classical and quantum predictions for frequencies at which a given amplitude F_0 yields the ionization quite fast on time scales of the order of few tens of the microwave period. For higher frequencies, the discrepancy between classical and quantum predictions appears. This behavior, as before, is qualitatively but not quantitatively (using a similar analysis as for the elongated states) consistent with the photonic localization theory [6].

Finally, Fig. 13 completes the study of elliptical states showing the ionization under the opposite polarization. The comparison of the amplitudes F_0 needed to produce similar $T(10\%)$ for right-hand and left-hand polarization in a similar absolute frequency range shows the asymmetry between the two possible polarizations. This asymmetry is of a classical origin—a phenomenon like this has been observed in the diffusive regime in the classical studies [30]. Note the strong increase of $T(10\%)$ for lower frequencies—we are approaching the limit of low frequencies with a relatively high threshold for the left-hand CPM [24,26,32].

It follows naturally that, as discussed on classical grounds in [30], close encounters with the nucleus (which are the main classical mechanism for the ionization in the LPM) play a small role for the CPM. The right-polarized microwave acting on the positive m_0 states only supplies the electron with additional angular momentum (due to the $\Delta m=+1$ selection rule). Therefore, the electron feels a centrifugal barrier and never comes close to the nucleus. For the opposite polarization of microwaves, when the angular momentum may diminish, the ionization is much less effective, which is definite proof that collisions with the nucleus are not important. No singularity of any type is observed in Fig. 8 near $m_0=0$, which again proves that encounters with the nucleus are not relevant for the ionization in the CPM.

D. Circular states

Finally, let us present results for circular states. As we have seen on the example presented in Fig. 8, these states may ionize at much higher microwave amplitudes than elliptical or elongated states. Thus the results presented below are of no relevance for the ionization threshold of atoms not preselected with respect to the angular momentum. However, efficient methods have been proposed [68] and confirmed experimentally [69] for preparing atoms in initial circular states. One may therefore envision a CPM ionization experiment in which atoms in circular states are prepared before entering the microwave cavity.

Figure 14 shows $T(10\%)$ thresholds obtained for different values of F_0 for circular states $n_0=48$, $m_0=48$ for moderate positive scaled frequencies. With increasing F_0, the curves shift to higher frequencies, indicating that the ionization yield decreases (in this frequency range) with ω_0. This agrees with the classical amplitude threshold $F(10\%)$ behavior, which, for circular states, increases also with frequency [30]. The dashed lines indicate classical time thresholds and show that the agreement between the classical and quantum predictions is strongly dependent on the time needed for reaching the threshold. For a strong field (at a given frequency), when 10% ionization is reached within up to approximately twenty cycles, the classical and quantum thresholds agree quite well. However, the quantum threshold rises much more sharply with the frequency and when the classical diffusion is slow (classical threshold of the order of a thousand cycles), the quantum threshold may exceed the classical value by several orders of magnitude.

The effect looks similar for different frequencies, but occurs simply at different microwave amplitudes. There is no quantitative difference between frequencies less and bigger than $\omega_0=1$— ''a starting point'' for quantum localization in

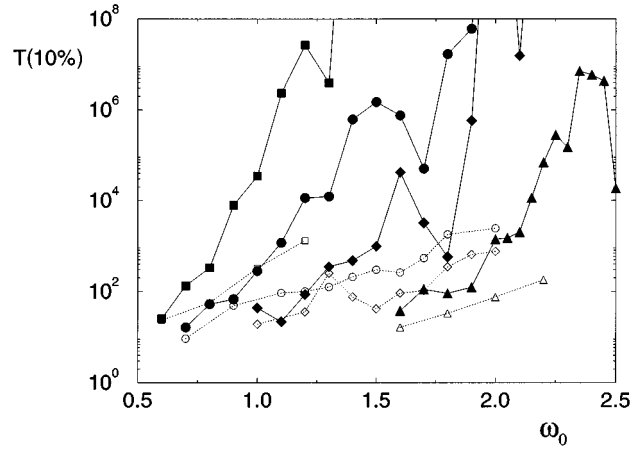

FIG. 14. $T(10\%)$ threshold for the initial circular state $n_0=48$, $m_0=48$ illuminated by a right-hand CPM for different scaled amplitudes F_0. The filled (open) symbols connected by lines give the quantum (classical) results. The squares, circles, diamonds, and triangles represent the data obtained for $F_0=0.02, 0.03, 0.04,$ and 0.07, respectively.

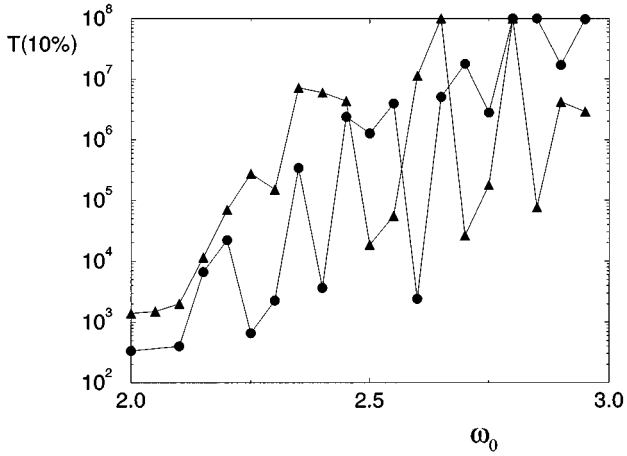

FIG. 15. $T(10\%)$ threshold for $F_0=0.07$ obtained for right-hand CPM ionization of circular state $n_0=48$, $m_0=48$ (filled triangles, cutoff $N=120$) and $n_0=64$, $m_0=64$ (filled circles, cutoff $N=160$).

the LPM studies [6,12]. One should, however, keep in mind that we are considering a situation that is outside the region of applicability of the photonic localization theory [see Eq. (6.1) above]. The observed behavior therefore may be quite different.

Looking along the vertical axis on the plot, it is clear that, for a given frequency, the changes of F_0 will determine whether the agreement between classical and quantum results occurs. For relatively small fields, there will be differences whereas for strong fields—leading to fast diffusion—we will find agreement between classical and quantum results. The region of slow classical diffusion is infested with remnants of regularities observed at still smaller microwave amplitudes (they create the obstacles slowing the diffusion). The classical transport in this case goes through several bottlenecks as studied in [70]. Thus a different mechanism leading also to quantum slowdown of the ionization process suggests itself. It has been proposed [71,72] that the finiteness of $\hbar$ leading to the ''coarse graining'' of the phase space will ''fill'' the gaps in broken tori and effectively slow down the quantum excitation leading to the discrepancies between classical and quantum mechanical results (or experimental results) observed in the LPM experiments [71]. Due to the structure of the classical phase space, this explanation of the origin of classical-quantum differences seems to be quite appropriate for the case of the CPM ionization of circular states.

Similar behavior occurs at larger scaled frequencies as shown in Fig. 15 for $F_0=0.07$ and in Fig. 16 for $F_0=0.1$. Both these figures show results for a larger initial principal quantum number $n_0=64$. The comparison with corresponding plots for elongated and in particular elliptical states reveals that the classical-quantum differences are more pronounced for circular states. This phenomenon may be understood qualitatively in terms of the dimensional argument. Extreme angular momentum states, $|n_0,m_0=n_0\rangle$, in right-hand polarized microwaves couple dominantly to n',m' states with large m' (remember the $\Delta m=+1$ selection rule for absorption). Hence the problem becomes effectively one dimensional. The situation is quite different if $m_0 \ll n_0$ since many more atomic states become coupled together, and we have a truly two-dimensional picture. The higher density of states for the elliptical initial state (not of all the atomic states, but of those important ones actively involved in the ionization process) means that the effective $\hbar$ becomes smaller. That means that the semiclassical limit is realized faster for the elliptical initial states and the quantum effect of gluing the holes in the regular phase space structures is smaller for these states.

As discussed above, on the average $T(10\%)$ increases quite sharply with ω_0 for a given F_0 in a whole interval corresponding to classically diffusive motion (i.e., up to $\omega_0 \approx 3-3.5$, beyond which the classical ionization thresholds increases sharply). To compare ionization at different frequencies on the same time scale, we have checked that in

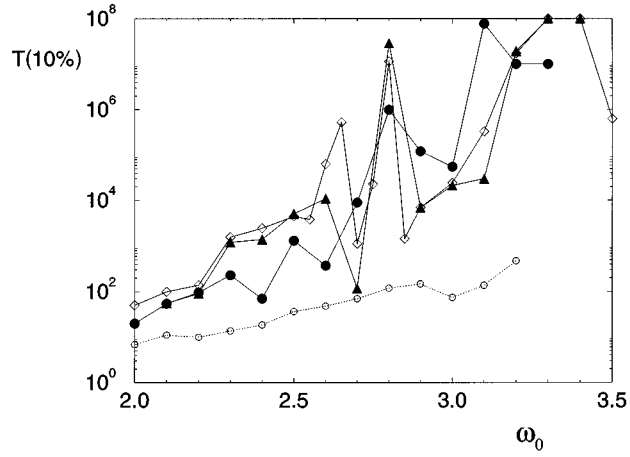

FIG. 16. Same as Fig. 15, but for stronger amplitude, $F_0=0.1$. The open diamonds represent the quantum data obtained also for the $n_0=48$, $m_0=48$ state, but for higher effective cutoff, $N\approx 151$—for some frequencies the shift of the cutoff strongly affects the value of $T(10\%)$. Note the classically scaling structure at $\omega_0 \approx 2.8$. Classical prediction is given by open circles connected by dotted line.

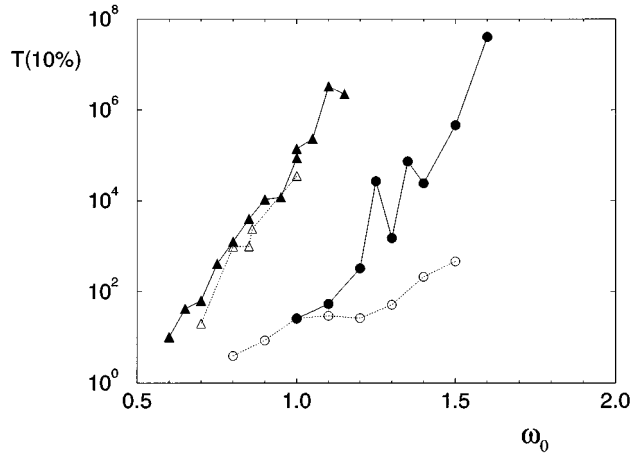

FIG. 17. Same as Fig. 15, but for left-polarized CPM (or right-polarized CPM for $n_0=48$, $m_0=-48$ state). Filled triangles, $F_0=0.15$; filled circles, $F_0=0.3$; the corresponding classical simulations are represented by open symbols. The required microwave amplitudes to obtain reasonable $T(10\%)$ values are much larger than those corresponding to right-polarized CPM—compare figures above.

the whole ''chaotic'' frequency region, the ionization process is quite similar statistically. For this purpose we used the width function $W(\varphi_0)$ defined as [63]

$$W(\varphi_0)=\exp\left\{-\sum_i \mathrm{Re}(\langle\tilde{\psi}_i|\varphi_0\rangle^2)\ln\mathrm{Re}(\langle\tilde{\psi}_i|\varphi_0\rangle^2)\right\} \tag{6.5}$$

closely related to the entropy and being a measure of the span of the initial state over the Floquet eigenstates. For the same purpose one may simply count the number of Floquet states (ordered in the descending order with respect to their overlap on the initial state) needed to exhaust the norm of $|\varphi_0\rangle$ up to say 99%. For similar values of the ionization probability and for a given pulse length (500 microwave cycles), the width function has similar values in the whole range of frequencies between $\omega_0=0.6$ and 2.6 and is a strongly increasing function of the ionization probability value chosen for comparison. In particular, $W\approx e^3$ for a 20% ionization during 500 microwave cycles corresponding to about 80 Floquet states needed to exhaust the norm of the initial state. For 1% ionization, we obtain $W\approx e^{1.5}$ with roughly 15 important Floquet states (note that the W function, while being roughly proportional to the number of important Floquet states in the expansion of the initial state, underestimates this number quite strongly). These numbers start to decrease significantly only for high frequencies when we come close to the classically forbidden region.

Finally, let us discuss the case of oppositely polarized microwaves presented in Fig. 17 as a function of ''negative'' frequency. One observes a very fast increase of the threshold time with absolute frequency value, even sharper than that demonstrated in Fig. 14. However, the microwave amplitudes used are roughly *one order of magnitude* higher than the corresponding values needed for right-polarized microwaves in the same frequency interval. This reflects the strong asymmetry between right-hand and left-hand polarized microwaves. Comparing the values of the field necessary to obtain reasonable $T(10\%)$ (see also Fig. 13), one notices that the asymmetry is much more pronounced for circular than for elliptical states (as expected since there should be no asymmetry of this kind for elongated states). Let us repeat that the effect (occurring at high frequencies, in contrast to the asymmetry of another origin at low frequencies [24,26,32]) is of a purely classical origin and has been discussed in detail in [30]. Also note the very good agreement between the classical and quantum predictions for $\omega_0<1$.

One should remember, however, that the quantitative predictions for the asymmetry may be dimension dependent and may be much smaller for a real 3D atom. It is precisely for circular orbits and negative frequencies where Nauenberg [21] observed the 3D atom to be less stable. Similar behavior was seen in classical simulations [30]. Still the asymmetry persists in the classical calculations also in the 3D model [30] and it should manifest itself quantum mechanically.

VII. CLASSICALLY SCALING STRUCTURES

While the classical time thresholds are quite smooth, the quantum results reveal several frequency-dependent structures. Some of them may be associated with incidental intermediate quantum resonances or the threshold effects (with increasing frequency fewer and fewer photons are required for ionization). These structures would not, however, scale classically. Therefore, they would occur at different values of the scaled frequency ω_0.

The comparison of the thresholds obtained for different n_0 reveals on the other hand a number of classically scaling structures, i.e., resonant features centered on the *scaled* frequency ω_0. Arguably the most prominent example appears for the circular states; note the structure present at frequency $\omega_0=2.8$ in Fig. 16. This local inhibition of ionization [manifested by the corresponding increase of $T(10\%)$] persists also for different ''effective ionization thresholds''—compare results for $n_0=48$ and $N=151$. Interestingly, even classical simulations show a slight slowdown of the ionization time in the vicinity of that frequency, confirming the classical nature of the resonance (although the effect is much weaker classically). For lower microwave amplitudes (compare Fig. 15) in the vicinity of $\omega_0=2.8$, the ionization is practically totally suppressed for both $n_0=48$ and 64.

Figure 15 yields another example. Note the locally increased $T(10\%)$ at $\omega_0=2.1$ appearing for $F_0=0.025$ for both $n_0=48$ and 64 circular states. The presence of such structures is dependent on F_0—it disappears for higher amplitude $F_0=0.04$ when $T(10\%)$ is much smaller. Such behavior is consistent with the proposed classical origin of the structure—for stronger microwave amplitude the remnants of regularity in the classical phase space become weaker and less significant.

Similarly, classically scaling structures appear for elliptical states as exemplified in Fig. 11 and Fig. 12 or for elongated states (compare Fig. 4). In the latter case, however, a slight shift in ω_0 of the resonance position with n_0 may be observed. As before, we believe that the observed structures are of classical origin and are related to structures in the

phase space, or more precisely, they correspond to localization of the Floquet states [contributing to the expansion in Eq. (4.2) in the dominant way] on the classical phase-space structures. The detailed study of the localization properties of Floquet states is beyond the scope of this paper and will be studied in [73].

VIII. SUMMARY AND CONCLUSIONS

We have presented extensive results for the ionization threshold dependence of the two-dimensional hydrogen atom illuminated by circularly polarized microwaves at realistic initial principal quantum numbers $n_0 \approx 50-60$ and for different initial angular momenta m_0. The results have been compared, whenever it was possible [i.e., for parameters within limits given by Eq. (6.1)], with the predictions of the photonic localization theory [6,67]. For elongated, high eccentricity states, quite nice qualitative agreement of our numerical results with that theory has been observed. However, theoretical predictions for the $F(10\%)$ threshold are systematically 2 times larger than the numerical results. In our opinion, a revision of the localization theory is needed. The localization theory seems to work quantitatively well for LPM [6,67]. The discrepancy observed for CPM indicates that the apparent similarity of atomic response to LPM and CPM for elongated states [23] may be valid in the perturbative regime only (i.e., only locally when the excitation of the atom is quite small).

It is worth stressing that the presented comparison with the photonic localization theory is the most complete to date. The dependence of the $F(10\%)$ prediction, Eq.(6.4), on all the parameters of the problem (ω_0, n_0, N) has been tested, confirming the functional form of Eq. (6.4) up to a constant discussed above.

The comparison of the ionization threshold dependence on the angular momentum with the predictions of the theory based on the Kepler map has shown significant differences, which, in our opinion, suggest that the regime of validity of the Kepler map approach and the photonic localization theory is more limited in the parameter space then anticipated originally [6]. This is in agreement with the classical discussion presented by Nauenberg [21]. His improved canonical Kepler map cannot be easily incorporated into the photonic localization theory to obtain the corrected quantum predictions. Such a development of the theory is therefore badly needed.

We have shown also, by a detailed study of classical-quantum correspondence for circular states (for which the photonic localization theory cannot be applied), the presence of strong localizationlike behavior in that case. We argue that the localization observed can be qualitatively explained by a quantum enhanced slowdown of the diffusion by remnants of regularities—the picture originally developed for the LPM ionization [71,72]. This is in agreement with the fact that the presence of classical-quantum differences is strongly dependent on the time scale on which the ionization occurs and only weakly on the frequency of the CPM. Note that such a picture can coexist with the photonic localization point of view. Further work is needed to clarify these points.

The asymmetry between thresholds observed for the left-hand polarized and right-hand polarized radiation and the fact that states of medium eccentricity are easiest to ionize confirm that the collisions with nucleus play a minor role in the CPM ionization of elliptical and circular states. This suggests that experimental verification of the results presented, for states of low eccentricity, may be carried out on an alkali rather than a hydrogen atom. Our viewpoint here is opposite to that expressed by Howard [23]. The existing experiments for rubidium in LPM [59–61] allow for both state selective preparation of the initial state and changes of the interaction time over several orders of magnitude. The only necessary modification is therefore the change of the microwave polarization.

The explanation of classical-quantum discrepancies as resulting from a quantum suppression of classical diffusion due to a partial localization on remnants of classical regularities is further confirmed by several observed classically scaling structures. We leave to a subsequent study a detailed analysis of these structures as well as the discussion of localization properties of important Floquet states in such cases.

ACKNOWLEDGMENTS

We have profited greatly from discussions with Andreas Buchleitner and Dima Shepelyansky. Laboratoire Kastler Brossel, de l'Ecole Normale Superieure et de l'Université Pierre et Marie Curie, is unité associée 18 du CNRS. CPU time on a Cray C98 and on a Cray YMP-EL has been provided by IDRIS and by the Centre de Calcul pour la Recherche de l'Université Pierre et Marie Curie. This work was supported by the Polish Committee of Scientific Research under Grant No. 2P302 102 06 (J.Z. and R.G.).

[1] See, e.g., D. Delande, in *Chaos and Quantum Physics 1989*, edited by M.-J. Giannoni, A. Voros, and J. Zinn-Justin, Les Houches Summer School Session LII (North-Holland, Amsterdam, 1991), p. 665.

[2] J. Zakrzewski, K. Dupret, and D. Delande, Phys. Rev. Lett. **74**, 522 (1995); K. Dupret, J. Zakrzewski, and D. Delande, Europhys. Lett. **31**, 251 (1995).

[3] J. E. Bayfield and P. M. Koch, Phys. Rev. Lett. **33**, 258 (1974).

[4] J. G. Leopold and I. C. Percival, J. Phys. B **12**, 709 (1979).

[5] G. Casati, B. V. Chirikov, D. L. Shepelyansky, and I. Guarneri, Phys. Rep. **154**, 77 (1987).

[6] G. Casati, I. Guarneri, and D. L. Shepelyansky, IEEE J. Quantum Electron. **24**, 1420 (1988).

[7] B. V. Chirikov, in *Chaos and Quantum Physics 1989* (Ref. [1]), p. 443.

[8] R. V. Jensen, S. M. Susskind, and M. M. Sanders, Phys. Rep. **201**, 1 (1991).

[9] A. Buchleitner, Thèse de Doctorat, Université Pierre et Marie-Curie, 1993 (in French) (unpublished).

[10] A. Buchleitner and D. Delande, Chaos, Solitons, Fractals **5**, 1125 (1995).
[11] A. Buchleitner, D. Delande, and J.-C. Gay, J. Opt. Soc. Am. B **12**, 505 (1995).
[12] P. M. Koch, in *Proceedings of the Eighth South African Summer School in Theoretical Physics: Chaos and Quantum Chaos, 13–24 January 1992, Blydepoort, Eastern Transvaal, Republic of South Africa* (Springer-Verlag, Berlin, 1993).
[13] P. M. Koch and K. A. H. van Leeuwen, Phys. Rep. **255**, 289 (1995).
[14] J. E. Bayfield and D. W. Sokol, in *Physics of Atoms and Molecules: Atomic Spectra and Collisions in External Fields*, edited by K. T. Taylor, M. H. Nayfeh, and C. W. Clark (Plenum, New York, 1988).
[15] M. V. Berry and K. E. Mount, Rep. Prog. Phys. **35**, 315 (1972).
[16] J. Mostowski and J. J. Sanchez-Mondragon, Opt. Commun. **29**, 293 (1979).
[17] B. I. Meerson, Opt. Spectrosc. **51**, 322 (1981) [Opt. Spektrosc. **51**, 522 (1981)].
[18] P. Fu, T. J. Scholz, J. M. Hettema, and T. F. Gallagher, Phys. Rev. Lett. **64**, 511 (1990).
[19] T. F. Gallagher, Mod. Phys. Lett. B **5**, 259 (1991).
[20] M. Nauenberg, Phys. Rev. Lett. **64**, 2731 (1990).
[21] M. Nauenberg, Europhys. Lett. **13**, 611 (1990).
[22] J. A. Griffiths and D. Farrelly, Phys. Rev. A **45**, R2678 (1992).
[23] J. E. Howard, Phys. Rev. A **46**, 364 (1992); **51**, 3934 (1995).
[24] K. Rzążewski and B. Piraux, Phys. Rev. A **47**, R1612 (1993).
[25] P. Kappertz and M. Nauenberg, Phys. Rev. A **47**, 4749 (1993).
[26] D. Delande, R. Gębarowski, M. Kuklińska, B. Piraux, K. Rzążewski, and J. Zakrzewski, in *Super-Intense Laser-Atom Physics*, Proceedings of NATO Advanced Workshop SILAP III, Han-sur-Lesse, Belgium, January 1993, edited by B. Piraux, A. L'Huillier, and K. Rzążewski (Plenum, New York, 1993), p. 317.
[27] R. Gębarowski and J. Zakrzewski, Phys. Rev. A **50**, 4408 (1994).
[28] M. J. Raković and S.-I. Chu, Phys. Rev. A **50**, 5077 (1994); **52**, 1358 (1995).
[29] D. Farelly and T. Uzer, Phys. Rev. Lett. **74**, 1720 (1995).
[30] R. Gębarowski and J. Zakrzewski, Phys. Rev. A **51**, 1508 (1995).
[31] Reference [30] contains the untrue claim of using for the first time a full regularization of Coulomb singularity in the microwave ionization problem. We would like to use this opportunity to point out that the same approach was used earlier by Griffiths and Farrely for the same problem [22] and introduced in the context of magnetized hydrogen atom by O. Rath and D. Richards, J. Phys. B **21**, 555 (1988).
[32] J. Zakrzewski, D. Delande, J. C. Gay, and K. Rzążewski, Phys. Rev. A **47**, R2468 (1993).
[33] D. Wintgen, Z. Phys. D **18**, 125 (1991).
[34] F. V. Bunkin and A. Prokhorov, Zh. Éksp. Teor. Fiz. **46**, 1090 (1964) [Sov. Phys. JETP **19**, 739 (1964)].
[35] A. Franz, H. Klar, J. T. Broad, and J. S. Briggs, J. Opt. Soc. Am. B **7**, 545 (1990).
[36] T. P. Grozdanov, M. J. Raković, and E. A. Solov'ev, J. Phys. B **25**, 4455 (1992).
[37] F. Benvenuto, G. Casati, and D. L. Shepelyansky, Phys. Rev. A **45**, R7670 (1992); **47**, R786 (1993).
[38] R. Gębarowski, Ph.D. thesis (in Polish), Jagiellonian University, Kraków, Poland, 1995 (unpublished).
[39] M. R. W. Bellermann, P. M. Koch, D. R. Mariani, and D. Richards, Phys. Rev. Lett. **76**, 892 (1996).
[40] H. Klar, Z. Phys. D **11**, 45 (1989).
[41] J. E. Howard, Phys. Rev. A **51**, 3934 (1995).
[42] I. Bialynicki-Birula, M. Kaliński, and J. H. Eberly, Phys. Rev. Lett. **73**, 1777 (1994).
[43] D. Farrelly, E. Lee, and T. Uzer, Phys. Rev. Lett. **75**, 972 (1995).
[44] D. Delande, J. Zakrzewski, and A. Buchleitner, Europhys. Lett. **32**, 107 (1995).
[45] J. Zakrzewski, D. Delande, and A. Buchleitner, Phys. Rev. Lett. **75**, 4015 (1995).
[46] A. Buchleitner and D. Delande, Phys. Rev. Lett. **75**, 1487 (1995).
[47] M. Kalinski and J. H. Eberly, Phys. Rev. A **52**, 4285 (1995).
[48] F. Benvenuto, G. Casati, and D. L. Shepelyansky, Phys. Rev. Lett. **72**, 1818 (1994).
[49] D. Farrelly, P. Bellomo, and T. Uzer, Phys. Rev. Lett. **74**, 3495 (1995).
[50] F. Benvenuto, G. Casati, and D. L. Shepelyansky, Phys. Rev. Lett. **74**, 3496 (1995).
[51] G. Floquet, Ann. Ecole Norm. Sup. **12**, 47 (1883); J. H. Shirley, Phys. Rev. **138**, B979 (1965).
[52] D. Delande, Thèse de doctorat d'état, Université de Paris, 1988 (in French) (unpublished).
[53] Obviously n_A+n_B must be even. The eigenbasis of 2D hydrogen in u,v coordinates is a subset of the full Hilbert space of the isotropic 2D harmonic oscillator. This is related to the properties of the dynamical symmetries of the isotropic 2D oscillator discussed in detail, e.g., in [52].
[54] W. P. Reinhardt, Annu. Rev. Phys. Chem. **33**, 323 (1982); Y. K. Ho, Phys. Rep. **99**, 1 (1983).
[55] S.-I. Chu and W. P. Reinhardt, Phys. Rev. Lett. **39**, 1195 (1977).
[56] A. Maquet, S.-I. Chu, and W. P. Reinhardt, Phys. Rev. A **27**, 2946 (1983).
[57] R. M. Potvliege and R. Shakeshaft, Phys. Rev. A **38**, 4597 (1988). M. Dörr, R. M. Potvliege, D. Proulx, and R. Shakeshaft, Phys. Rev. A **43**, 3729 (1991).
[58] J. Zakrzewski and D. Delande, Phys. Rev. E **47**, 1665 (1993).
[59] M. Arndt, A. Buchleitner, R. N. Mantegna, and H. Walther, Phys. Rev. Lett. **67**, 2435 (1991).
[60] R. Blümel, A. Buchleitner, R. Graham, L. Sirko, U. Smilansky, and H. Walther, Phys. Rev. A **44**, 4521 (1991).
[61] O. Benson, A. Buchleitner, G. Reichel, M. Arndt, R. N. Mantegna, and H. Walther, Phys. Rev. A **51**, 4862 (1995).
[62] A. Buchleitner, D. Delande, J. Zakrzewski, R. N. Mantegna, M. Arndt, and H. Walther, Phys. Rev. Lett. **75**, 3818 (1995).
[63] R. Blümel and U. Smilansky, Z. Phys. D **6**, 83 (1987).
[64] H. P. Breuer, K. Dietz, and M. Holthaus, Z. Phys. D **18**, 239 (1991).
[65] M. Gajda, B. Piraux, and K. Rzążewski, Phys. Rev. A **50**, 2528 (1994).
[66] D. Delande, A. Bommier, and J. C. Gay, Phys. Rev. Lett. **66**, 141 (1991).
[67] G. Casati, I. Guarneri, and D. L. Shepelyansky, Physica A **163**, 205 (1990).

[68] D. Delande and J. C. Gay, Europhys. Lett. **5**, 303 (1988).
[69] J. Hare, M. Gross, and P. Goy, Phys. Rev. Lett. **61**, 1938 (1988).
[70] R. S. MacKay, J. D. Meiss, and I. C. Percival, Physica **13D**, 55 (1984).
[71] R. S. MacKay and J. D. Meiss, Phys. Rev. A **37**, 4702 (1988).
[72] J. D. Meiss, Phys. Rev. Lett. **62**, 1576 (1989).
[73] J. Zakrzewski and D. Delande (unpublished).